Progress in Oceanography 224 (2024) 103263

https://doi.org/10.1016/j.pocean.2024.103263

Potential impacts of offshore wind energy development on physical processes and scallop larval dispersal over the US Northeast shelf

Changsheng Chen, Liuzhi Zhao, Huichan Lin, Pingguo He, Siqi Li, Zhongxiang Wu, Jianhua Qi, Qichun Xu, Kevin Stokesbury, Lu Wang

School for Marine Science and Technology, University of Massachusetts Dartmouth, New Bedford, MA 02744, USA

A B S T R A C T

This study examines the potential impact of offshore wind energy facilities on the local and regional circulation, stratification, and scallop larval dispersal and settlement over the U.S. Northeast continental shelf. A coupled high-resolution (up to ~ 1.0 m), wind turbine-resolving hydrodynamical (NS-FVCOM) and scallop individual-based (Scallop-IBM) model was employed. Comparisons were made for scenarios with and without wind turbine generators (WTGs), encompassing three-dimensional flow fields, water temperature, bottom stress/vertical mixing, scallop larval dispersal, settlement, and distributions. The interaction of M_2 tidal currents with monopiles generates significant horizontal flow shear on the downflow lee side. The fluid–structure interaction-induced mesoscale currents deviate substantially from the idealized flow fields examined typically in the device-scale laboratory or coarse-grid hydrodynamical models with subgrid-scale explicit parametrizations. Stratification induces noteworthy changes in the flow around individual monopiles throughout the water column, with the maximum bottom stress primarily oriented in the onshore-offshore direction and vertical eddy viscosity occurring around all directions of individual monopiles. The deployment of a WTG array amplifies offshore low-frequency subtidal flow around 40 to 50-m isobaths, forming mesoscale eddies over the shelf. This enhanced flow contributes to offshore water transport, redirecting scallop larvae toward the Nantucket Lightship Closed Area (NLCA). The accumulation of larvae in the NLCA is attributed to eddy-induced retention.

1. Introduction

A significant concern within the fishing community revolves around the potential impact of mesoscale flow generated by offshore wind energy facilities on water transport and mixing over the southern New England Shelf (NES). This concern stems from the potential repercussions on scallop larval transport, settlement distribution, and, consequently, overall abundance and landings of scallops in the U.S. Northeast.

The U.S. northeast continental shelf is a vital support system for numerous fisheries. Notably, sea scallops (*Placopecten magellanicus*) harvested in this region contribute approximately 28% of global scallop production (Naidu and Robert, 2006; Shumway and Parson, 2016; NFSC, 2018). Annually, New England witnesses the landing of over $500 million worth of sea scallops, totaling around 50 million pounds (Larsen and Lee, 1978; Stokesbury and Bethoney, 2020). Similar to many marine living resources, scallop fishery stocks face challenges posed by envi-ronmental changes and exploitation pressure, leading to fluctuations in fishery landings (Hart, 2006; Hart and Chute, 2004; Hart and Rago, 2006; Davies et al., 2015).

Despite sea scallops being a sedentary species with limited migratory ability (Posgay, 1981; Melvin et al., 1985), their pelagic larvae are easily advected by ocean currents, establishing an effective connection be-tween geographically separated populations from Georges Bank (GB) to the southern Mid-Atlantic Bight (MAB) (Tremblay et al., 1994; Gallager et al., 1996; Chen et al., 2021a). Given the influence of flow variability on sustaining high scallop concentration and providing a dispropor-tionately large number of recruits to the commercial fishery, there is apprehension that offshore wind energy development could alter flow patterns, potentially impacting regional scallop population and recruits.

The Bureau of Ocean Energy Management (BOEM) mandates a thorough assessment of the impact of prospective wind energy facilities on small-scale coastal (local) and regional offshore physical and biological environmental processes. Addressing local small-scale considerations necessitates a state-of-the-art coupled atmospheric-ocean-physical model with a horizontal resolution capable of discerning the geometric scale of individual wind turbines. In response to BOEM's requirements, we developed a wind turbine-resolving, high-resolution (up to ~ 1.0 m) subdomain FVCOM ocean model within the offshore wind farm development regions in Massachusetts (MA) and Rhode Island (RI) waters. This subdomain model was nested with the Northeast Coastal Ocean Forecasting System (NECOFS), enabling the linkage of regional

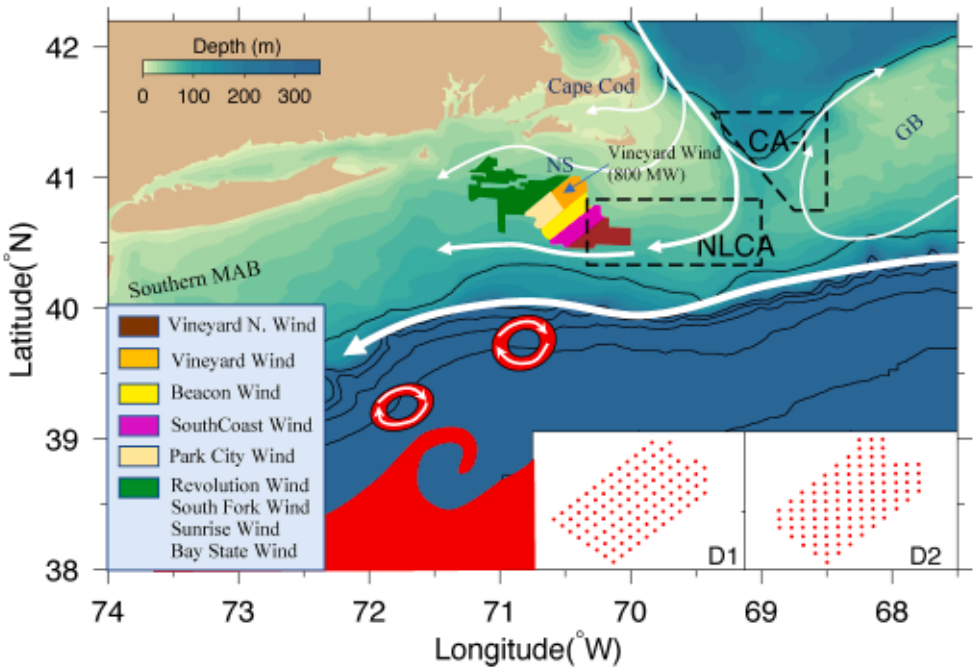

Fig. 1. The leasing areas in the federal waters of Massachusetts and Rhode Island overlapped with the schematic pattern of the flow from the Cape Cod coast on the north and southern Georges Bank on the east (the white arrows) and eddies from the Gulf of Stream (red color rings). Heavy dashed lines represent the closed areas in the Great South Channel (CA-I) and the Nantucket light (NLCA). The right-lower panels are the layout designs (D1 and D2) proposed initially by *Vineyard Wind LLC*. (For interpretation of the references to color in this figure legend, the reader is referred to the web version of this article.)

ocean responses to locally induced changes by wind turbines.

Selecting a hundred-year extratropical storm (Nor'easter in February 1979) and Hurricane Bob in August 1991 as scenarios, we executed the nested model for cases with and without the inclusion of 136 wind turbines covering the entire BOEM-approved MA and RI lease areas. Our assessment focused on investigating the impact of future offshore wind energy resource development on surface waves, circulation, water transport, and bottom stress across local and regional scales (Chen et al., 2016a). A key finding of our study revealed that during storms, the environmental changes induced by the wind turbine facility exhibited spatial and temporal variations in response to alterations in wind in-tensity and wind direction fields. Despite these changes, our simulations, based on a 5–6 nautical miles (nm) monopile separation scale, indicated that fish larvae could navigate through the offshore wind turbine areas during storms without significant impediments. However, it is note-worthy that current industry standards mandate a 1-nm separation scale between monopiles. This raises the crucial question of how the current and planned 1-nm monopile separation layout may potentially impact local and regional environmental changes, specifically its effects on the transport and distribution of fish and shellfish larvae.

Nantucket Shoals is a flow-through region characterized by two distinct water sources: the southward flow from the Cape Cod coast and the westward flow from the southern Georges Bank (GB) and shelf break (Fig. 1) (Shearman and Lentz, 2003). The water flowing through the southern NES maintains its southward trajectory toward the southern MAB. Additionally, Nantucket Shoals is identified as a high tidal energy dissipation area (Shearman and Lentz, 2004), where the southward- propagating tidal energy flux from the western Gulf of Maine (GOM) along Cape Cod meets the northeastward tidal energy flux from the NES (Chen et al., 2011). The pivotal question revolves around the potential impact of offshore wind facilities on the western side of this region on the tidal energy flux in the convergence zone. Specifically, the inquiry aims to understand whether such facilities could alter the tidal energy flux from the NES and subsequently influence sediment distribution in Nantucket Shoals. The presence of wind turbines, potentially acting as barriers, prompts consideration of whether they may generate mesoscale or even small-scale eddies and currents within and around the wind energy area. Consequently, the question centers on whether the turbine-induced flow could enhance vertical and horizontal mixing, leading to potential alterations in sediment transport and distribution. Given the critical dependence of scallop larval settlement and recruitment on their habitat, it becomes imperative to assess the potential impacts of offshore wind energy facilities on local and regional environments. This question underscores the need for an assessment that aims to provide optimal design options, striking a balance between the nation's renewable energy development goals and the sustainability of commercial fisheries.

The MAB, spanning from Cape Cod, MA, in the north to Cape Hatteras, NC, in the south, is known for its characteristic "cold pool" near the bottom during spring through fall (Lentz, 2017). This cold pool emerges with the seasonal development of the thermocline in spring, creating a favorable environment for fisheries, particularly scallops. Concerns have been raised by Miles et al. (2021) regarding potential changes in stratification due to offshore wind farm development that could impact the seasonal formation and degradation of the cold pool, consequently affecting fishery production in the region.

The northeast coastal communities are grappling with the impacts of climate change, particularly the effects of heatwaves and rising sea levels on storm-induced coastal inundation, coastal ecosystems, and fisheries. The growing concern is that these impacts will be exacerbated by increasing global warming in the U.S. Northeast region (Chen et al., 2021a). The warming trend is evident in the satellite-derived sea surface temperature (SST) change over the U.S. northeastern shelf in recent decades (Fig. 2), with a significant warming event occurring in 2012. The warming rate of the SST averaged over the shelf bounded at the 300- m isobath was approximately 0.04 °C/year from 1982 to 2020. Assuming 2012 as a year for warming regime shift, the mean SST sub-sequently rose by about 1.0 °C compared to the climatological SST mean averaged over 1982–2011.

This warming trend is captured in the NECOFS. The warming rate exhibits significant spatial variation, with the maximum warming observed around the shelf break off GB. As detected in the NECOFS-

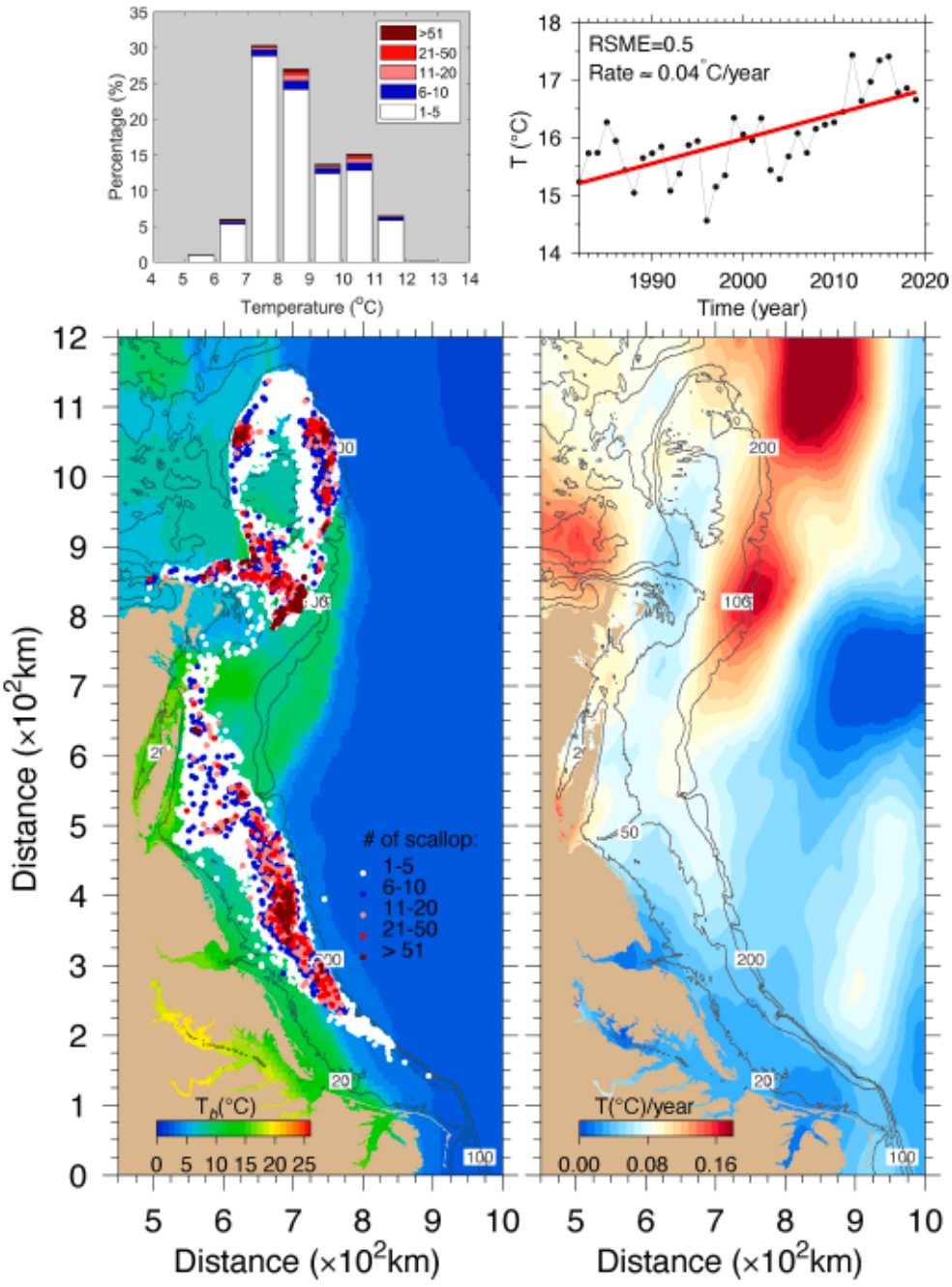

Fig. 2. Upper-right panel: The yearly Sea Surface Temperature (SST) increase rate over the period 1982–2020. This rate was estimated based on satellite-derived SST data in the region shown in the lower-right panel. Solid black dots represent the yearly averaged SST for each year, while the thick red line indicates the linear regression fitting line. Lower-right panel: The distribution of the yearly SST increase rate averaged over the period 1982–2020. Upper-left panel: Observed scallop abundance versus autumn-mean bottom water temperature sampled over the northeast U.S. continental shelf from 1978 to 2016. Lower-left panel: The spatial distribution of scallops overlapped with NECOFS-simulated autumn-mean bottom water temperature in the U.S. Northeast over the period 1978–2016. (For interpretation of the references to color in this figure legend, the reader is referred to the web version of this article.)

simulated temperature and flow fields, the warming has intensified the cross-isobath gradient of water temperature on the southern flank of GB, consequently strengthening the clockwise gyre over the bank. When combining multi-source scallop abundance data with NECOFS-assimilated bottom temperatures over the period 1978–2017, a high geographic correlation between bottom temperature and scallop abundance distribution is evident (Fig. 2). Given that bottom temperature is a primary factor directly impacting scallop growth in the benthic stage, regional warming may play a crucial role in the scallop recruitment. Moreover, warming is anticipated to enhance water stratification, resulting in a thinner surface ocean mixed layer (OML). Chen et al. (2021a) highlighted that the settlement of scallop larvae is significantly influenced by larval behaviors in the OML. The thin OML tends to reduce the larval retention in the water column. An essential question emerges: How will the impact of warming change after the development of offshore wind farms in the region? This question remains unexplored, particularly using a wind turbine-resolving, high-resolution coupled physical and fishery model.

In 2018, the BOEM granted approval for *Vineyard Wind LLC's (VW)* Site Assessment Plan (SAP) within the lease area of OCS-A-0501. *VW* proposed the installation of up to 100 wind turbine generators (WTGs), each with a capacity ranging from 8 to 10 megawatts (MW) (OCS EIS/

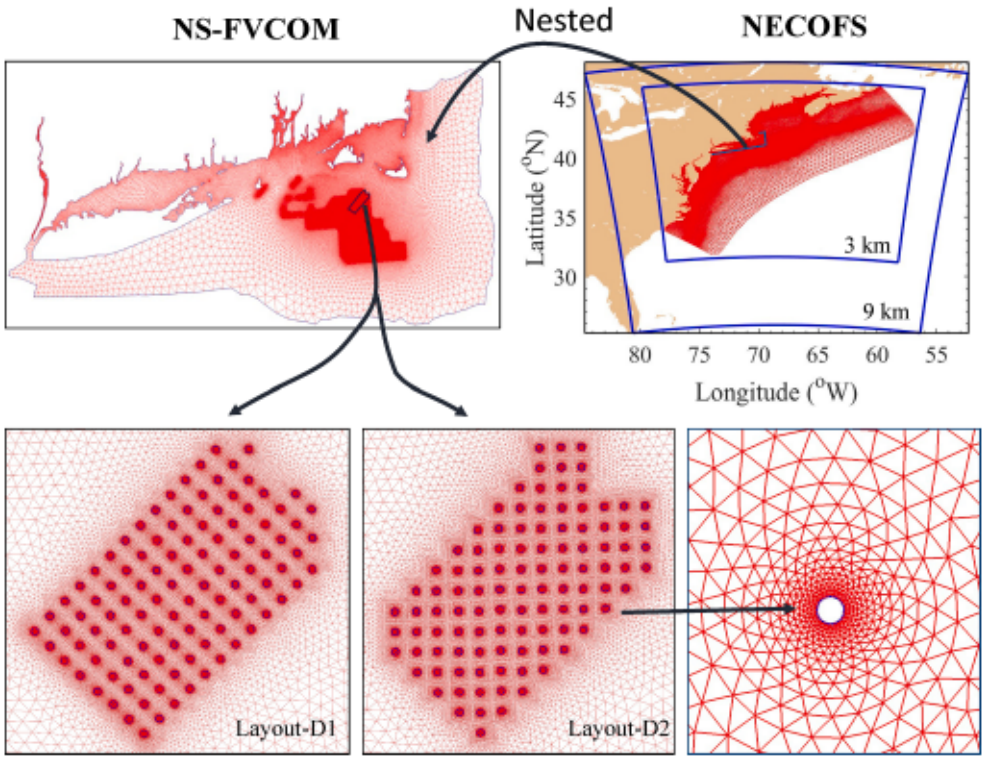

Fig. 3. The model grid of wind turbine-resolving regional- NECOFS and local subdomain NS-FVCOM coupled model system. Upper left panel: NECOFS, an atmospheric (WRF)-ocean (FVCOM) coupled model system. Blue boxes: Nested domains 1 and 2 for WRF. Red mesh: FVCOM grid with a horizontal resolution up to ~ 100 m. Upper right: The subdomain NS-FVCOM grid with a horizontal resolution up to ~ 1.0 m. Black box: the *Vineyard Wind LLC*'s lease area of OCS-A-0501. Lower left and middle panels: Enlarged views of the model grids designed based on layouts D1 and D2. Lower-right panel: An enlarged view of the grid around a monopile. (For interpretation of the references to color in this figure legend, the reader is referred to the web version of this article.)

EA, BOEM2018-060). The proposed layout included two alternatives, D1 and D2, with a separation spacing of approximately 0.75–1.0 nm between individual WTGs (Fig. 1). In the D1 layout, WTGs were planned to be aligned in a northwest-southeast orientation, while the D2 layout featured an east–west alignment. The towers of WTGs have diameters of approximately 20 feet (~6.1 m) and 28 feet (~8.5 m), respectively. *VW* proposed to mount individual WTGs with either a monopile foundation or a Jacket (Pin piles) foundation. For monopiles, the proposed foun-dation diameter size ranged from a minimum of 25 feet (~7.5 m) to a maximum of 34 feet (~10.3 m). In the case of Pin piles, the proposed foundation diameters varied from 5 feet (~1.5 m) to 10 feet (~3.0 m).

Offshore wind turbines form a complex three-dimensional habitat, resembling intentionally constructed artificial reefs. Studies in Europe, as well as research on the Block Island Wind Farm (BIWF) off RI, USA, have documented a rapid growth of marine life following wind farm construction (Carey et al., 2020). Encrusting organisms like mussels and barnacles, along with structure-loving fish species such as tautog and black seabass, are often attracted to these structures. In Europe, re-searchers observed an increase in the density of piscivorous groundfish, such as Atlantic cod, and reef-associated species, like goldsinny wrasse, in close proximity to the foundations of wind farms one year after installation (Bergstrom et al., 2013). They also noted that hard substrate from scour protection created new habitats for species that preferred such conditions (Van Hal et al., 2017). Since 2019, ongoing research has been conducted to assess the potential impact of wind farms on fisheries resources off the south coast of MA and RI. The research employs various methods, including trawl surveys, drop camera optical imaging, lobster pot surveys, and surveys focusing on highly migratory species (e.g., Rillahan and He, 2021). These surveys aim to collect data before and after wind farm constructions, facilitating impact evaluation through the Before-and-After-Impact (BACI) analysis (Underwood,1991; Sto-kesbury et al., 2023). Wilber et al. (2024) utilized a meticulously designed BACI sampling strategy to evaluate the influence of the BIWF on lobster catches. Their findings revealed a 30% decrease in lobster catches near the wind farm and an 18% reduction at a reference location compared to pre-construction levels. However, for the wind farm over Nantucket Shoal, data for the after-construction period is unavailable, and the impact on fisheries resources remains unknown. Significantly, prior to this study, no fine-scale modeling had been executed to project potential changes in fisheries.

Building upon the success of developing the nested NS-FVCOM and NECOFS system, we extended our efforts by coupling NS-FVCOM with a scallop individual-based model (Scallop-IBM) (Chen et al., 2021b). Using the VW's lease area OCS-A-050 as a pilot site, we extensively examined the impacts of offshore wind farm development on local and regional flow fields, mixing via stratification, and scallop larval trans-port and settlement over the southern NES. The model simulations comprehensively considered the wind and heat flux changes induced by WTGs, two layout designs, and anticipated climate change.

This paper concisely summarizes the primary findings derived from the modeling assessment results. The subsequent sections are organized as follows. Section 2 details the models and numerical designs employed in our studies. Section 3 presents the results of model simulations, encompassing (a) the atmospheric and ocean environment changes induced by WTGs and b) the impacts of WTGs, layout designs, and climate change on scallop larval dispersal and settlement. Section 4 elucidates the physical processes attributed to the changes in regional water transports induced by the WTG array and underscores the areas that necessitate future exploration to understand the cumulative impact of WTGs on the region. Finally, section 5 synthesizes the findings and provides concluding remarks.

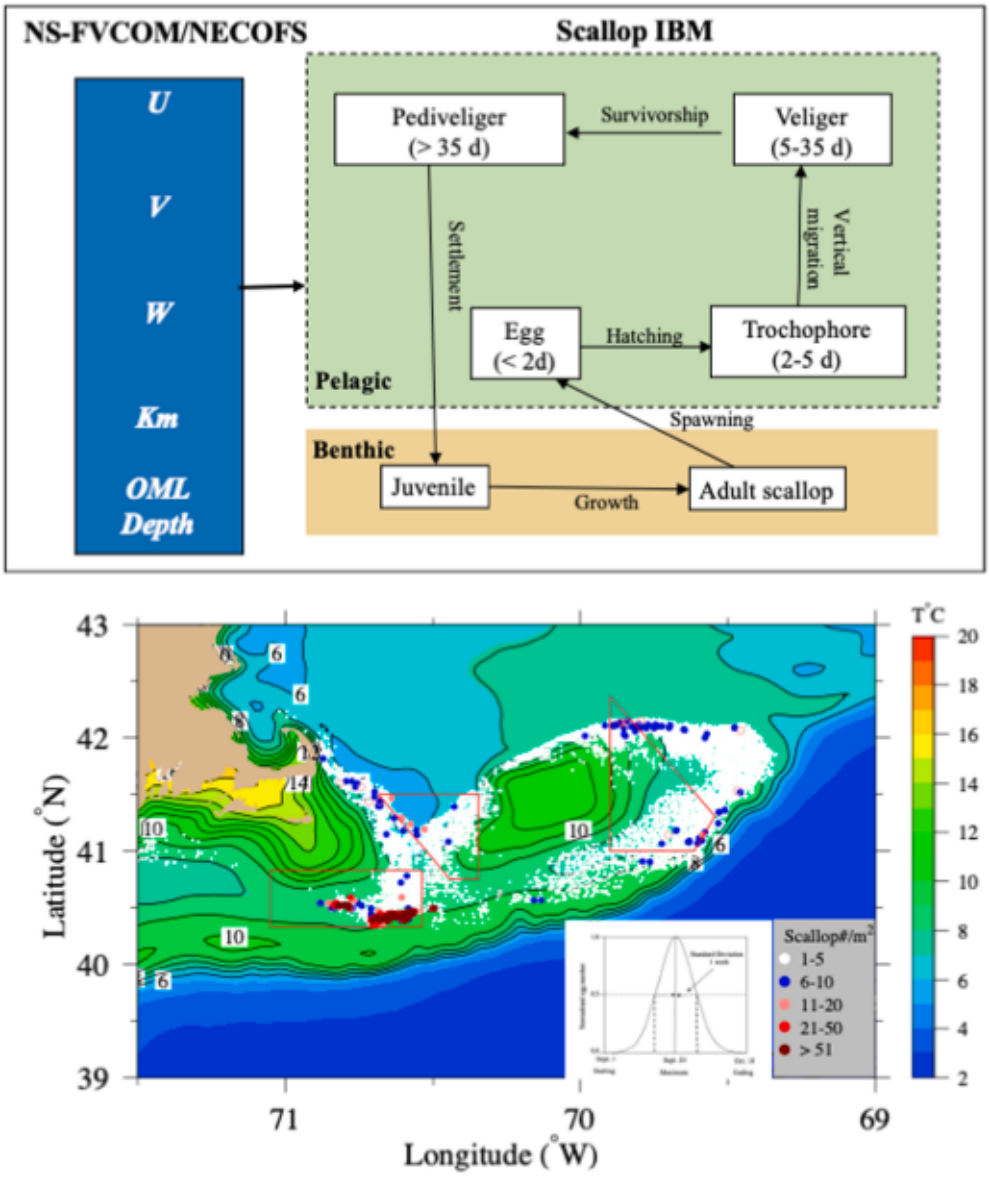

Fig. 4. Upper panel: structures of the scallop-IBM model encompassing four pelagic stages (egg, trochophore, veliger, and pediveliger). Lower panel: the spatial distribution of scallops overlapped with bottom water temperature, taking into account spawning over Georges Bank and the Great South Channel. The shapes bounded by red lines indicate the closed areas. The figure inserted in the right-lower corner illustrates the egg spawning period starting at 00:00 on September 1 and ending at 24:00 on October 10. The spawning process follows a normal probability distribution with a peak on September 20 and a standard deviation of one week. (For interpretation of the references to color in this figure legend, the reader is referred to the web version of this article.)

2. The models and numerical designs

The assessments utilized an updated coupled model system comprising a wind turbine-resolving, local–regional nested hydrodynamic model known as NS-FVCOM/NECOFS and an individual-based scallop population model known as Scallop-IBM. NECOFS stands as an integrated atmosphere, surface wave, and ocean forecast model system designed for the northeast U.S. coastal region. The upgraded computational domain of NECOFS encompasses the entire northeastern shelf, stretching from Cape Hatteras to the Scotian Shelf, inclusive of the southern MAB (Fig. 3). The existing regional-domain system consists of three key components: 1) a community mesoscale meteorological model named "Weather Research and Forecasting (WRF-AWR)" (https://www2.mmm.ucar.edu/wrf/users/download/get_sources.html), 2) the regional ocean model of FVCOM (Chen et al., 2003, 2006, 2013a), and 3) the unstructured-grid surface wave model (FVCOM-SWAVE), modified from SWAN (Qi et al., 2009), sharing the same domain as FVCOM. The ocean model in the upgraded NECOFS has evolved into a global-regional-river nested system, incorporating the Gulf Stream-shelf interaction (*e.g.*, warm-core rings), volume and mass transports entering the U.S. Northeast over the Nova Scotia shelf from the upstream Lab-rador Sea or even the Arctic Ocean (Chen et al., 2016b; Zhang et al., 2016a, 2016b, Zhang et al., 2020a), and river discharges from the Water Balance Model (WBM) or National Water Model (NWM). NECOFS has undergone validation through comparisons with numerous available observations spanning the last 41 years (1978–2018). These validations encompass water levels (Chen et al., 2011), stratification (Li et al., 2015), currents (Sun et al., 2016; Cowles et al., 2008), extreme events such as hurricanes, extratropic storms, surges, and coastal inundations (Beardsley et al., 2013; Chen et al., 2013b; Sun et al., 2013; Li et al., 2020; Li and Chen, 2022), and the impacts of the sea level rise on storm- induced coastal inundations (Zhang et al., 2020b; Chen et al., 2020).

NS-FVCOM is a subdomain wind turbine-resolving ocean model nested through the boundary to NECOFS. The computational domain of

NS-FVCOM encompasses the shelf regions off MA, RI, Block Island, Block Island Sound, and Long-Island Sound (Fig. 3). This model was initially configured to assess the potential impact of offshore wind facilities in the BOEM-issued lease areas in the waters of MA and RI, including the five operated WTGs on the eastern shelf of Block Island. The configuration of WTGs was upgraded by including the two layout designs proposed by *VW* in the lease area of OCS-A-0501. To resolve WTGs, we configured NS-FVCOM with a horizontal resolution of ~ 1.0 1.3 m around the WTG tower (Fig. 3). Even -levels (10 layers) with a uniform thickness were specified in the vertical, maintaining a reso-lution of 4 m on the 40-m isobath and up to about 0.5 m on the 5-m isobath. This vertical resolution was sufficient to resolve the vertical stratification in the lease area of OCS-A-0501 (Chen et al., 2021b).

NS-FVCOM was driven by surface forcing (wind stress, surface heat flux plus short-wave irradiance, precipitation minus evaporation) with lateral boundary conditions specified through one-way nesting with the regional FVCOM. The regional FVCOM provided the initial and boundary conditions for hydrodynamics variables (sea level, velocity, temperature, salinity, horizontal diffusion coefficient, and vertical eddy viscosity). The surface forcing data were provided by the WRF model (Grell, 1993). In NECOFS, the WRF model was configured with a regional domain (covering the Northeast U.S.) and a local domain (covering the Scotian Shelf, GOM, GB, and NES) with a horizontal grid spacing of 9.0 and 3.0 km, respectively. In this study, we considered two types of WRF forcing for the cases with and without considering the wind and heat flux changes due to WTGs. In the case with WTGs, we utilized the sub-grid-scale WTG power curve module available in WRF by adding a 1.0-km subdomain (Fitch et al., 2012). The parameteriza-tions used in the turbine-resolving WRF simulation were based on *VW* s proposed installation plan with a turbine hub height of 121 m, a rotor diameter of 180 m, a turbine nominal power of 10 MW, and a standing thrust coefficient of 0.13. NS-FVCOM can be operated under either hy-drostatic or non-hydrostatic conditions. In this study, we utilize the hydrostatic approximation.

Scallop-IBM, as previously delineated in our prior publication (Chen et al., 2021a), comprises four pelagic phases: egg, trochophore, veliger, pediveliger, and benthic stage with feeding, predation, starvation, resuspension, and natural/fishing mortality (Tian et al., 2009a, 2009b, 2009c; Chen et al., 2021a) (Fig. 4). During pelagic phases, develop-mental stages are classified based on age: eggs 2 days, trochophores 2 4 days, veligers 5 40 days, and pediveligers 40 days (Stewart and Arnold, 1994; Pearce et al., 2004; Cragg, 2006). The model relies on fixed development times for pelagic stages, assuming that minor inter-annual changes in water temperature insignificantly influence larval development times. Similarly, we disregard food limitation, pre-supposing ample food availability during pelagic stages.

The response of scallop larvae to light, currents, turbulence levels, and oceanic mixing are well-documented for each behavior-life stage. Our approach to modeling larval behavior and vertical migrations is grounded in an observational understanding of each life stage. For instance, eggs, spawned on the seabed, neutrally drift passively via vertical currents and turbulence without vertical migration (Culliney, 1974). Trochophores exhibit random spinning without directional swimming (Tian et al., 2009a) and are consequently treated passively. Once the larvae form the first shell (*prodisoconch*), they swim upwards across the thermocline because the gravity centers are below the velum (Gallager, 1993). Veligers experience horizontal drift in the surface Oceanic Mixed Layer (OML) above the thermocline, actively switching between upward swimming and sinking, resulting in a distinct vertical migration pattern. Sensitivity to light transitions, rather than prolonged light intensity states like day or night, influences veliger behavior (Gallager et al., 1996). Larvae aged between 5 and 40 days exhibit various vertical migration patterns within the OML, such as thermocline-seeking diel or semidiurnal cycling (Tremblay and Sinclair, 1990a; Tremblay and Sinclair, 1990b; Gallager et al., 1996; Manuel et al., 1996). Observations and laboratory mesocosm experiments supported such diel and semidiurnal migration cycles (Tremblay and Sinclair, 1990b; Manuel et al., 1996). Larvae also respond to turbulence pulses greater than 10^{-7} W/kg by withdrawing their velum and sinking rapidly until the turbulent energy subsides (Pearce et al., 1998).

Table 1
Types of Physical Model Experiments.

Cases	Physical Model	Physical model resolution	WRF forcing	WRF resolution
Case 1	NECOFS-FVCOM	Up to ~ 100 m	WRF without considering the wind change due to WTGs	3 km
Case 2	NS-FVCOM without WTGs	Up to ~ 1.0 m	WRF without considering the wind change due to WTGs	1 3 km
Case 3	NS-FVCOM with WTGs	Up to ~ 1.0 m	WRF without considering the wind change due to WTGs	1 3 km
Case 4	NS-FVCOM with WTGs	Up to ~ 1.0 m	WRF with considering the wind and heat flux changes due to WTGs.	1 3 m

Throughout the benthic phase, age undergoes incremented changes at each time step, while shell height and weight evolve through simulations driven by trophodynamics and metabolism. Starvation mortality is intricately linked to metabolism and food assimilation, where an inadequate supply of assimilated food to meet metabolism energy consumption leads to mortality due to starvation. Food sources include phytoplankton, biogenic detritus, and suspended terrestrial sediment. Each food compartment is characterized by a distinct nutritional value, parameterized as a growth efficiency coefficient. Suspended sediments, although lacking nutritional value, play a crucial role in interfering with the scallop s filtration performance. This compartment is designed to address the impact of suspended terrestrial detritus on the scallop s food intake system, as well as the filtration clogging that arises at elevated concentrations of suspended matter.

This paper focuses specifically on the pelagic stages, while the results regarding the impacts of offshore wind farm facilities on scallop recruitment during the benthic stages will be presented in a separate paper. Scallop-IBM was driven by the merged physical fields of NS- FVCOM and NECOFS. The larval tracking equations used in Scallop- IBM were detailed by Chen et al. (2021a). The simulation incorpo-rated diel and semidiurnal vertical migration behaviors in the OML during the pelagic stages. Various physical conditions were provided by the NS-FVCOM experiments, as outlined in Table 1. Adult sea scallops undergo spawning over GB and the Great South Channel (GSC) areas (Fig. 4) during fall (Posgay and Norman,1958). In alignment with the methodology employed by Chen et al. (2021a), the scallop spawning pattern was annually defined, with a modeled normal distribution starting at 00:00 GMT on September 1 and ending at 24:00 GMT on October 10 (Fig. 4). Notably, the peak spawning period was set on September 20, with a 1-week standard deviation. The primary spawning event, accounting for 95 % of total spawning, spanned four weeks. This timeframe aligns with field measurements as reported by Posgay and Norman (1958), Posgay (1976), Mullen and Morning (1986), and DiBacco et al. (1995). The simulation was conducted annually, with the Scallop-IBM model integrated over three months from September 1 to November 30. This timeframe accommodates a larval settlement time scale of approximately 40 days.

Numerical experiments were done for selected years 2009, 2010, and 2013, chosen based on the percentage of larvae settled over GB/GSC, southern NES, and the southern MAB in the last 39 years from 1978 to 2016 (Chen et al., 2021a). In 2009, a notable southward larval transport occurred from GB/GSC to the NES and the southern MAB. In 2010, there was abundant larval settlement in the *VW* s leased area. Additionally, the water temperature in the U.S. Northeast has seen a significant in-crease since 2012, and we selected 2013 to represent the warming

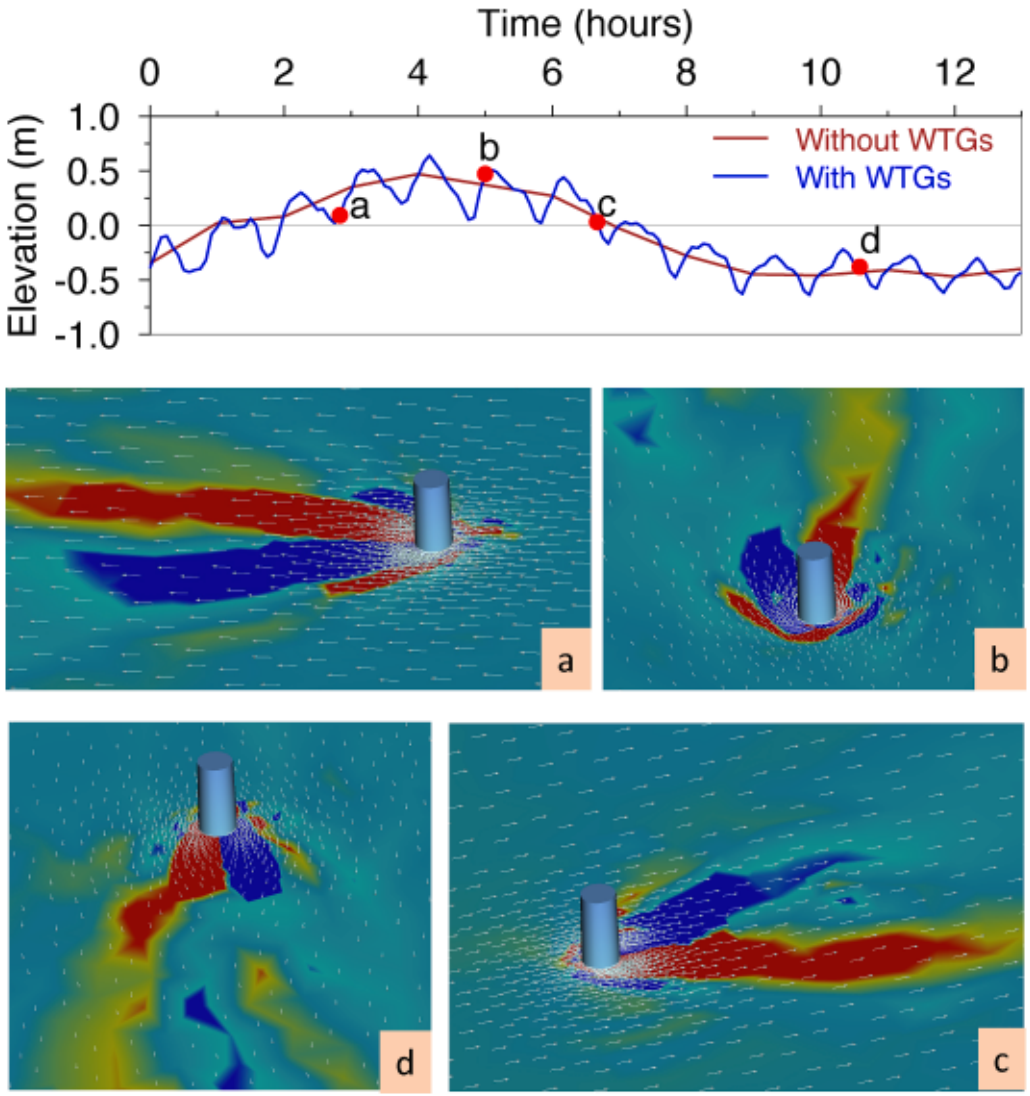

Fig. 5. Color images: enlarged views of the vorticity field overlapped over the surface current vectors (red: positive; blue: negative) around a monopile at four phases (a: the westward flow; b: transition from the westward to northward flow; c: eastward flow, d: transition from the eastward to southward flow) over a semidiurnal M_2 tidal cycle. Vectors: near-surface currents. Upper panel: changes in water elevations near the monopile for the cases without and with WTGs. Red dots marked by labels "a, b, c, and d" were when the images were selected. The fluid-monopile interactions produced a high-frequency variation in the elevation with a period of approximately one hour. (For interpretation of the references to color in this figure legend, the reader is referred to the web version of this article.)

period. Four types of physical model experiments were conducted (Table 1), with a simulation period covering three months, from September 1 to November 30. For the Case 1 experiment, the NECOFS-FVCOM covered the entire U.S. Northeast. To compare the scenarios with and without WTGs, Cases 2 and 3 experiments were conducted by running the NS-FVCOM with the same resolution of up to ~ 1.0 m. Furthermore, the impact of the wind and heat flux changes due to WTGs on the physical environment was examined through the Case 4 experiment.

3. The simulation results

3.1. Changes in physical fields

The primary results from the NS-FVCOM experiments with WTGs demonstrate that monopiles can considerably enhance the eddy circulation and velocity shear or vorticity within and around the turbine area (Fig. 5). In such an M_2 tidal currents-dominant and stratified region (Lentz et al., 2003), the interactions of tidal currents with monopiles generated complex patterns of the horizontal flow shear on the downflow lee side of individual WTGs. The downstream maximum horizontal velocity shear rotated clockwise with the M_2 tidal current, during which the eddy shedding appeared almost randomly as shear instability occurred. The water movement within the WTG array, resulting from the fluid–structure interaction, represented a significant departure from either the idealized flow fields driven generally by uniform, steady freestream flow in the device-scale laboratory or Computational Fluid Dynamics (CFD) studies or the flow pattern predicted by coarse-grid hydrodynamical models with subgrid explicit wind turbine parameterizations (Johnson et al., 2021).

In the scenario with WTGs (see Fig. 5; upper panel), we observed a high-frequency oscillation, approximately a one-hour period, in both surface elevation and currents. This oscillation, which overlapped with the M_2 tidal cycle, was stimulated by tidal-dominant flow around individual monopiles and associated with internal waves. Further examination is needed to understand the underlying physical mechanisms.

The vortex wake is a widely recognized phenomenon in fluid dynamics, particularly when studying the flow around a circular cylinder (Schlichting, 1979). In scenarios without friction, the fluid undergoes acceleration on the upstream side and deceleration on the downstream

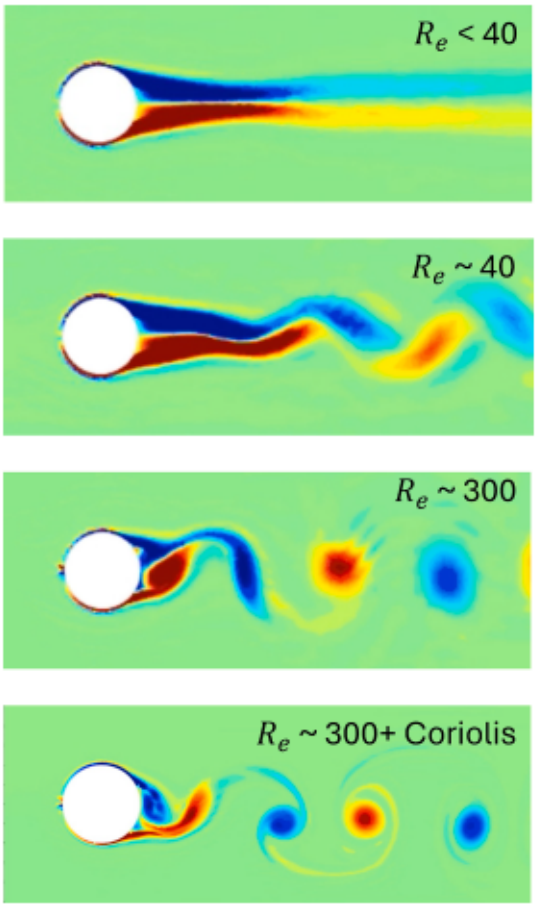

Fig. 6. Vorticity fields simulated from FVCOM vortex wake experiments with a steady flow around an idealized circular island. Experiments were done for the cases with Reynold numbers (R_e) of < 40, ~40, ~300, and ~ 300 plus Coriolis. The transition from laminar flow to a Kármán vortex street appears when R_e > 40. The vortex shedding becomes asymmetric when a constant Coriolis frequency ($f = 10^{-4}$ s^{-1}) is added.

side, resulting in a separation point at the midpoint. As the Reynolds number (Re), calculated as the product of flow speed and characteristic length divided by kinematic viscosity, increases, the initially laminar flow transforms into a Kármán vortex street on the lee side (Chang, 1970). In the hydrodynamic equation, Re reflects the ratio of the horizontal advection term to the diffusion term, with the vortex wake occurring when the advection significantly outweighs diffusion.

Before applying FVCOM to simulate wind turbine-induced flow, we conducted validation experiments to confirm its capability to generate a vortex street downstream of an individual monopile. These experiments involved subjecting an idealized circular island to a steady flow within a broad, flat-bottom channel. The outcomes affirm that FVCOM's unstructured-grid finite-volume algorithm faithfully reproduces the transition from laminar flow to a vortex street under conditions where Re exceeds 40 (refer to Fig. 6). Introducing a constant Coriolis frequency ($f = 10^{-4}$ s^{-1}) results in asymmetric vortex shedding.

Remarkably, the simulated vorticity field around individual monopiles showed no discernible regular vortex wake. This suggests that the clockwise-rotating M_2 tidal currents and wind-induced mixing did not create conducive conditions for a well-defined vortex street in the offshore wind farm region.

CFD models were utilized to establish drag coefficient and eddy viscosity parameterization within the offshore wind farm area for a regional hydrodynamics model configured with a turbine-unresolvable grid. This approach was instrumental in assessing the impact of offshore wind facilities on the regional marine environments (Johnson et al., 2021). The wind turbine-resolving NS-FVCOM simulation results indicate a notable temporal and spatial variability in the vorticity field from turbine to turbine. Resolving such variability through parameterization presents a significant challenge.

Nantucket Shoal was stratified during the fall season. The flow around an individual WTG varied significantly throughout the water column, particularly during flood and ebb tidal periods. An illustrative example is presented in Fig. 7, depicting the distributions of the near-surface and near-bottom currents around a randomly selected WTG in the center of the array. When the near-surface flow was westward, the near-bottom flow exhibited a distinct northwestward direction (Fig. 7a), with a flow direction difference of approximately 70° or more. Conse-quently, the maximum velocity shear on the downstream lee side appeared at the surface on the west, but at the bottom on the northwest side. A similar phenomenon occurred during the ebb tidal period, where the downstream lee side was situated to the south for the near-surface flow, and to the east for the near-bottom flow (Fig. 7d). This disparity diminished during the M_2 tidal current transition period (Fig. 7b, c). The vertical structure of the stratified flow posed a challenge to be resolved through the subgrid-scale parameterization, necessitating the use of a wind turbine-resolving model.

We computed the mean and maximum bottom stress, as well as vertical eddy viscosity for the scenarios involving WTGs over September-November of 2009, 2010, and 2013 (Fig. 8). The variations in bottom stress predominantly manifested in the onshore-offshore direction, with a three-month mean peak value reaching up to 0.15 N/m^2. During storm periods, the maximum bottom stress around individual WTGs could soar to 2.0 N/m^2, approximately ten times greater than the seasonally averaged value. The alteration in vertical eddy viscosity occurred throughout the water column surrounding individual WTGs in all directions. However, the intensification was confined to a narrow area within a 5-m range around monopiles. Storms induced energic mixing around a monopile. Owing to the absence of a convection mechanism in the hydrostatic approximation, the model-simulated maximum eddy viscosity experienced a sudden increase during storms. Turning on the nonhydrostatic dynamics is crucial to accurately capture the mixing physics around WTGs, particularly under stratified conditions.

We conducted a comparative analysis of the variation in the maximum bottom stress over a regional scale between the scenarios with and without WTGs. The observed significant changes were found to be contingent on wind intensity and direction, primarily within the lee side areas of WTGs. While the regional distributions of the bottom stress remained consistent between the cases with and without WTGs, the downwind impact extended across a relatively expansive area. The maximum difference reached up to 0.2 N/m^2 around the 50-m isobath (Fig. 9: upper panels). In a closer inspection focused on the WTG array, the disparity in bottom stress varied from one wind turbine to another, exhibiting positive or negative values within the range of < 0.05 N/m^2 (Fig. 9: lower panels).

Similar features were observed in the vertically averaged viscosity. Variations between the scenarios with and without WTGs were contingent on wind intensity and direction. A notable distinction was evident in the lee side areas of WTGs, with the maximum impact extending around the 50-m isobath (Fig. 10: upper panels). Upon closer examination of the WTG array, it was apparent that the sign of the difference in vertical viscosity significantly fluctuated from one WTG to another (Fig. 10: lower panels). The maximum positive value was concentrated around the outer edge area of the WTG array, although its magnitude was considerably less than 0.01 m^2/s.

The NS-FVCOM simulation incorporated tidal and wind forcings. To further understand the individual contributions of these forcings, we conducted an additional experiment by excluding wind forcing. This allowed us to quantify the relative impact of the interactions of wind and tidal-driven currents with monopiles on changes in vertical viscosity and bottom stress. The results revealed that, for the changes in vertical

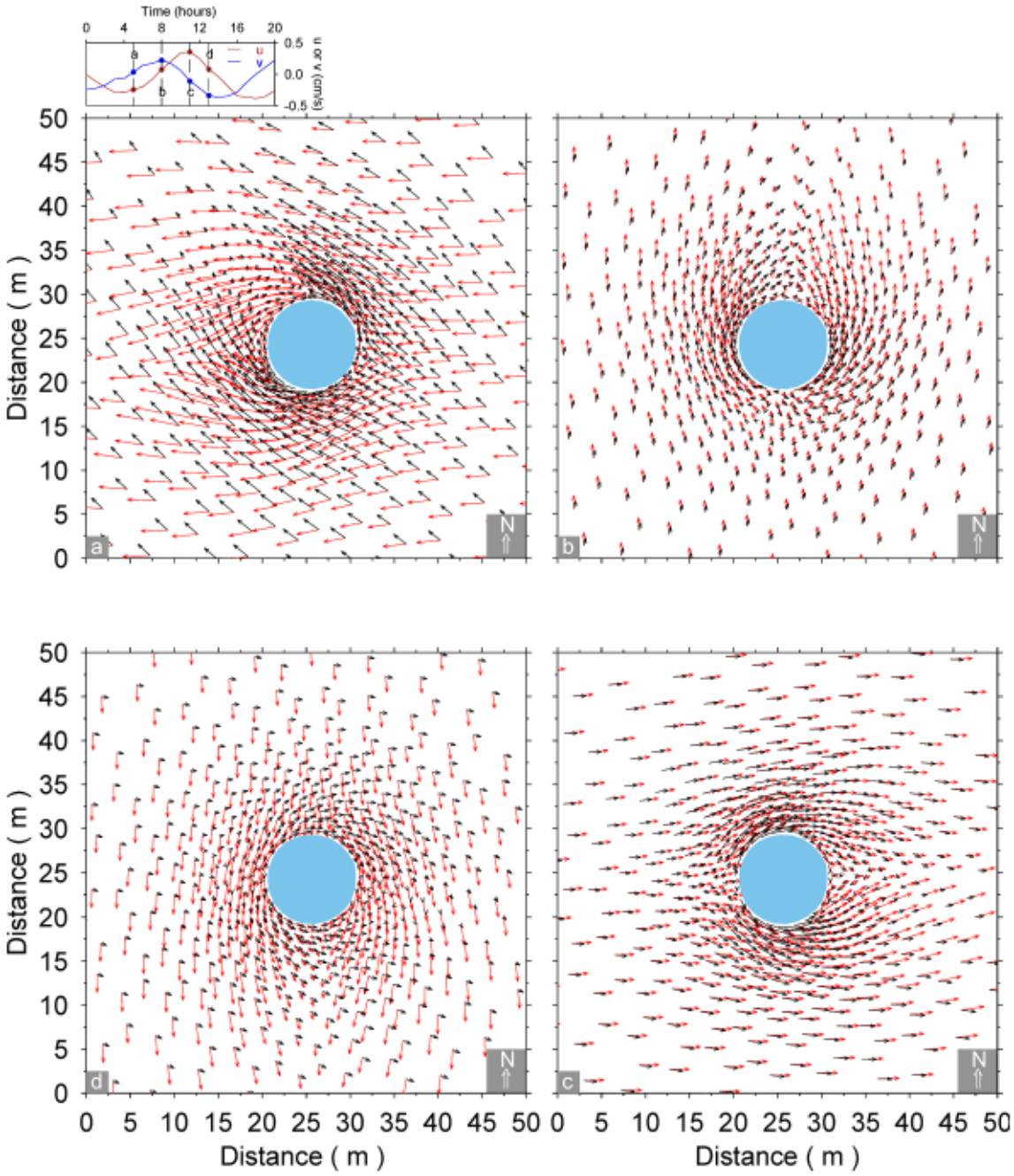

Fig. 7. The distributions of the near-surface (red color vectors) and near-bottom (black color vectors) around a monopile at four phases (a: the westward flow; b: transition from the westward to northward flow; c: eastward flow, d: transition from the eastward to southward flow) over a semidiurnal M_2 tidal cycle. The top-left plot presents the locations of a, b, c, and d over an M_2 tidal cycle, where u and v are the east- and north components of the near-surface hourly velocity near the monopile. Eastward and northward: positive. (For interpretation of the references to color in this figure legend, the reader is referred to the web version of this article.)

viscosity, the interaction of wind-driven currents with monopiles accounted for approximately 33 % around individual monopiles and about 55 % in the broader region. Regarding bottom stress, the contribution was about 53 % around individual monopiles and 48 % over the regional scale.

The alteration in bottom stress and vertical viscosity induced by WTGs had a direct impact on the regional water temperature. As an illustrative case, we selected the year 2013 to compare the monthly averaged temperature differences at the surface and bottom between the scenarios with and without WTGs. Our findings revealed that the extent of influence due to WTGs varied with both wind intensity and direction (Fig. 11). In September, a period characterized by stratified water, the temperature difference was more pronounced at the bottom than the surface (Fig. 11: left column). The maximum influenced areas were concentrated in the downwind lee side region, with a broader influence observed at the surface compared to the bottom. While the temperature change due to WTGs was less than 0.5 °C at the surface, it reached 1.0 °C around the 50-m isobath at the bottom. In October, vertical mixing gradually intensified as the wind strength increased. The distributions of the WTGs' influenced areas on temperature between the surface and bottom were similar (Fig. 11: middle column). The maximum difference occurred in the downwind lee side, reaching a maximum of < 1.0 °C near the 50-m isobath. In November, characterized by considerably strengthened wind speed and variable wind direction, enhanced

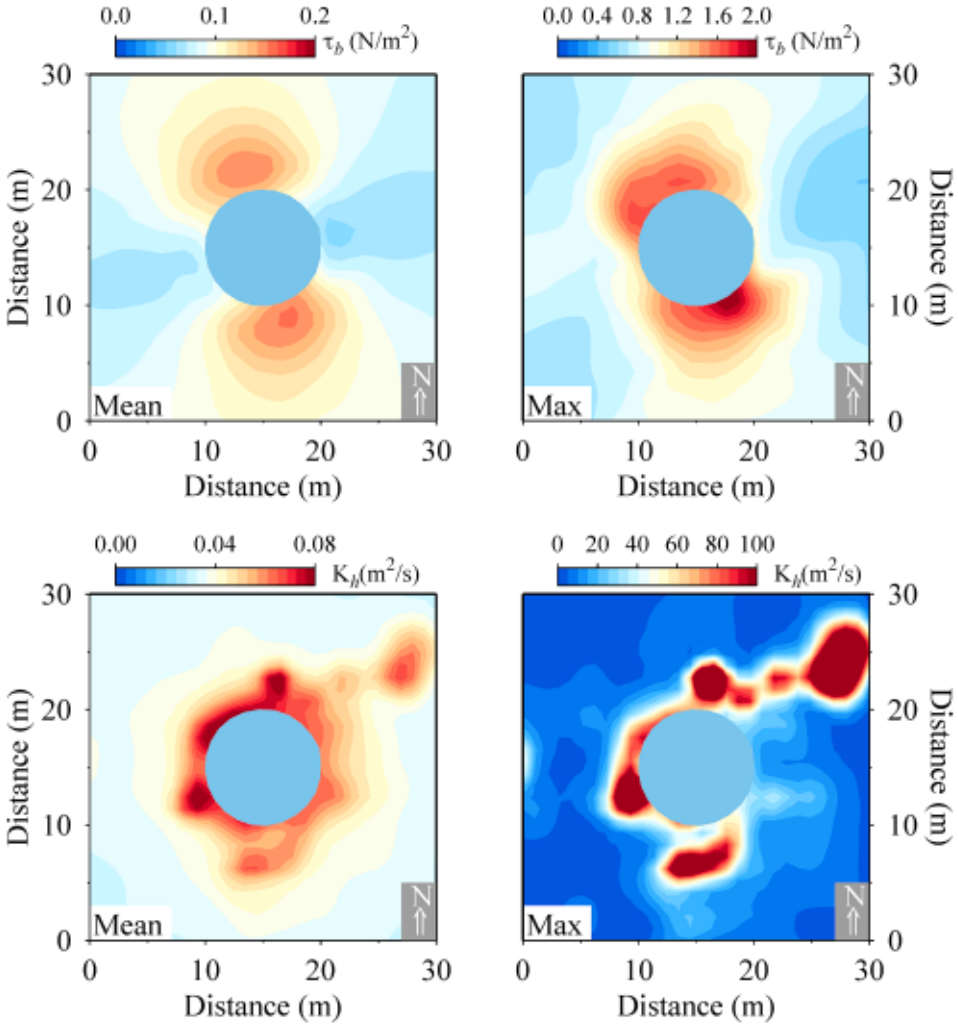

Fig. 8. Distributions of mean and maximum bottom stresses (upper panels) and vertical thermal diffusion coefficients (lower panels) around a monopile over September-November. 2009, 2010, and 2013.

advection and mixing around WTGs significantly expanded the influenced temperature area at the surface. The temperature difference was at a level of 1.0 °C or even larger.

3.2. Changes in scallop larvae dispersal and settlement

3.2.1. Experiments disregarding the impact of WTGs on winds and heat fluxes

The comparisons of super individuals and larvae densities between the cases with and without WTGs revealed a significant alteration in larval transport due to changes in the flow field within the deployed WTGs' area in 2009, 2010, and 2013. Throughout these three years, the flow tended to push the larvae offshore from September to November. An illustrative example is presented in Fig. 12 for the year 2013. We observed a notable reduction in horizontal dispersion within and around the wind energy development area., resulting in the offshore advection of numerous scallop larvae into the Nantucket Lightship Closed Area (NLCA). While larval behaviors played a critical role in larval dispersal and settlement by modifying the flow-induced advection at different depths, they did not alter the WTG-induced enhancement of the offshore larval transport in that particular year. This characteristic remained consistent for 2009 and 2010 as well.

Dividing the model domain into 2 × 2 km boxes, we conducted a statistical analysis of the mean, percentage, and standard deviation of the ensembled larval density for the cases with and without WTGs over 2009, 2010, and 2013 (Fig. 13). This calculation accounted for semi-diurnal and diel vertical migration behaviors. The percentage was defined as the ratio of settled years to the total ensembled years in individual boxes. Considering diel and semidiurnal migration cases, the total ensembled years are 6. The settled years indicated the years in which larvae successfully settled in a specific box. Changes in the flow field induced by WTGs tended to aggregate larvae and transfer them offshore as a cohesive group. Consequently, the deployment of WTGs in the lease area significantly increased the mean larval abundance in the NLCA compared to a scenario without WTGs. The settling percentage in the NLCA experienced a notable rise of 20–40 % when considering the presence of WTGs. The existence of WTGs also reduced the spatial de-viation of ensembled larval density, with a maximum variation occur-ring within the NLCA.

3.2.2. Experiments incorporating the impact of WTGs on winds and heat fluxes

We examined the influence of downwind wake on oceanic currents and scallop larval transport by considering the impact of WTGs on winds and heat fluxes. As an illustrative case, we selected the year 2013 and conducted a re-run of the high-resolution (1.0 km) WRF, incorporating the sub-grid WTG power curve module as outlined by Fitch et al. (2012). The parameterizations applied in the turbine-resolving WRF were based on *VW*'s proposed installation plan, featuring 10 MV WTG towers with a turbine hub height of 121 m, a rotor diameter of 180 m, and a standing

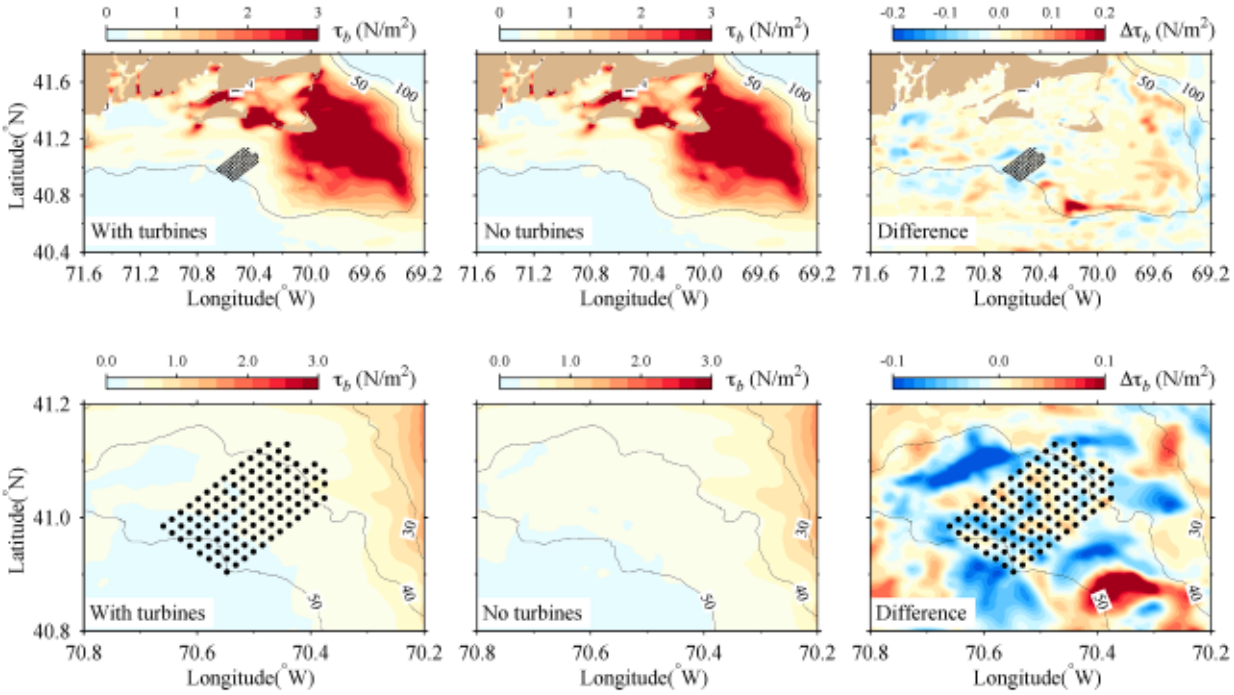

Fig. 9. Upper panels: Maximum bottom stresses and their difference over September to November 2009, 2010, and 2013 for the cases with and without wind turbines. Lower panels: Zoom-in views of the upper panel figures around the wind turbine array area.

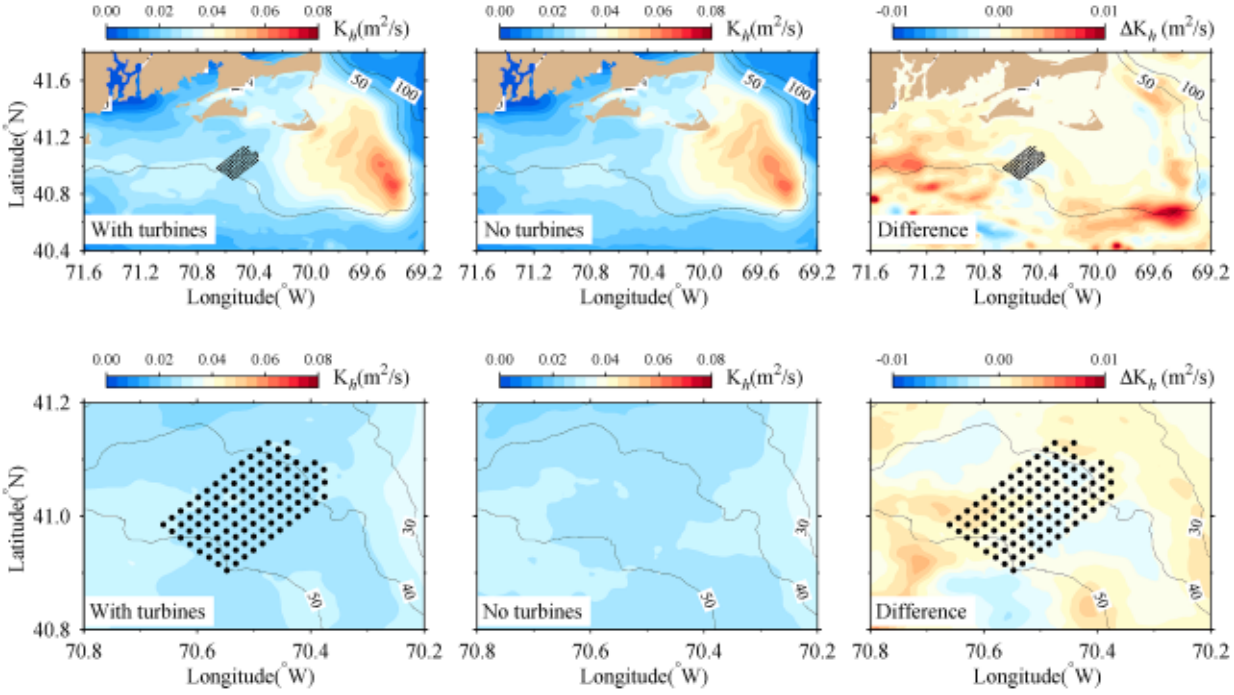

Fig. 10. Upper panels: Vertically averaged mean thermal diffusion coefficients and their difference over September to November 2009, 2010, and 2013 for the cases with and without wind turbines. Lower panels: Zoom-in views of the upper-panel figures around the wind turbine array area.

thrust coefficient of 0.13. The impact of the downwind wake on the wind intensity and direction exhibited significant seasonal variations (Fig. 14). The most pronounced alterations occurred on the lee side in areas corresponding to the seasonally dominant wind directions: southeastern in spring, northeastern in summer through fall, and southeastern in winter. The magnitude of these changes correlated with wind intensity, reaching its maximum during winter. However, despite the potential of WTGs to generate a substantial downwind wake at the hub height, their influences on the surface wind were notably diminished. The maximum change in wind speed attributed to WTGs at the 10- m height was 0.2–0.3 m/s, primarily during winter, and a directional shift of 1.0–1.2° in direction, occurring predominantly in summer through autumn.

The downwind wake increased the spatial variation of oceanic currents, consequently altering the movement of scallop larvae. This alteration resulted in a significantly different distribution of the settled

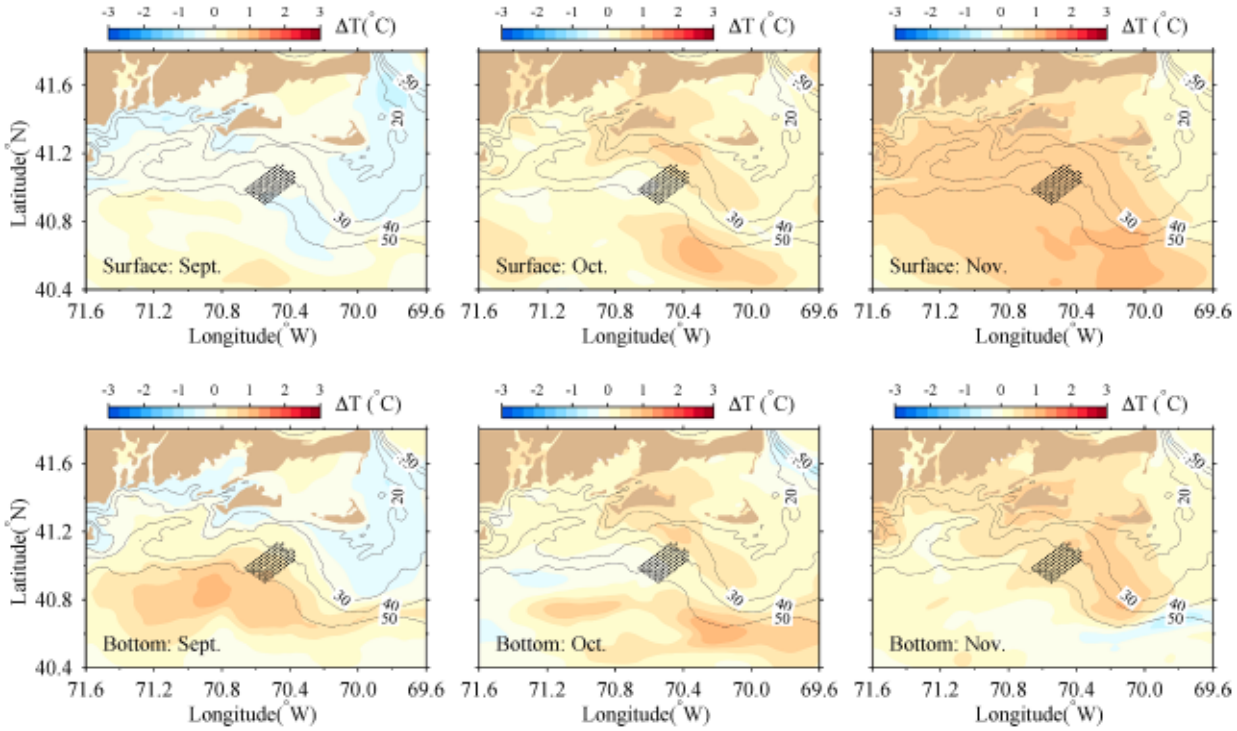

Fig. 11. The surface (upper) and bottom (lower) temperature differences averaged over September, October, and November 2013 for the cases with and without wind turbines.

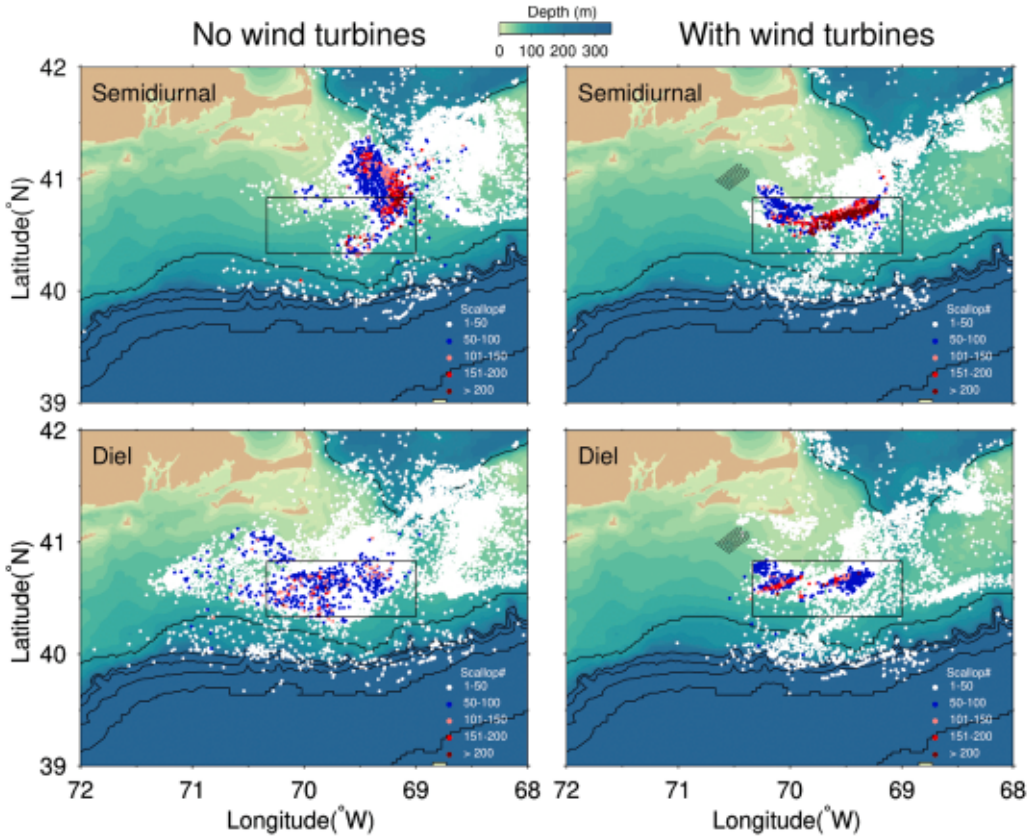

Fig. 12. Locations and abundances of settled super-individual scallop larvae in the southern New England region for the cases with and without wind turbines on November 30, 2013. Experiments were done for semidiurnal (upper) and diel (lower) larval migration behaviors. The black box: the Nantucket Lightship Closed Area. Black dots: the monopile's locations.

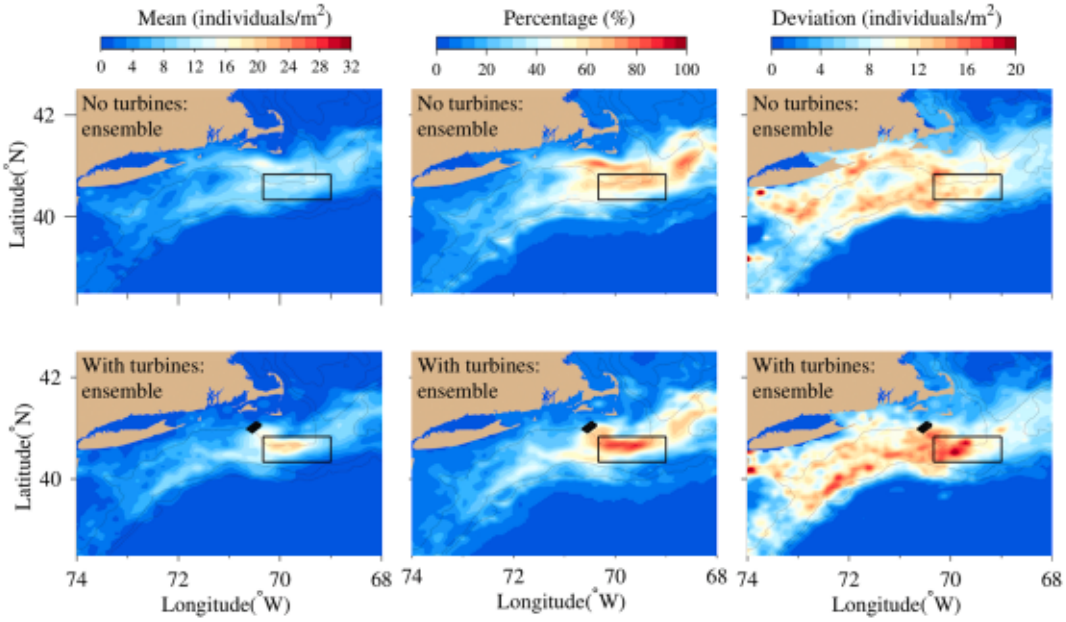

Fig. 13. The swimming behavior-ensembled, means, percentages, and standard deviations of settled scallop larvae over 2009. 2010, and 2013 for the cases without (upper panels) and with (lower panels) wind turbines. Black lines are the 50, 100, and 200-m isobath contours. The black box is the Nantucket Lightship Closed Area (NLCA).

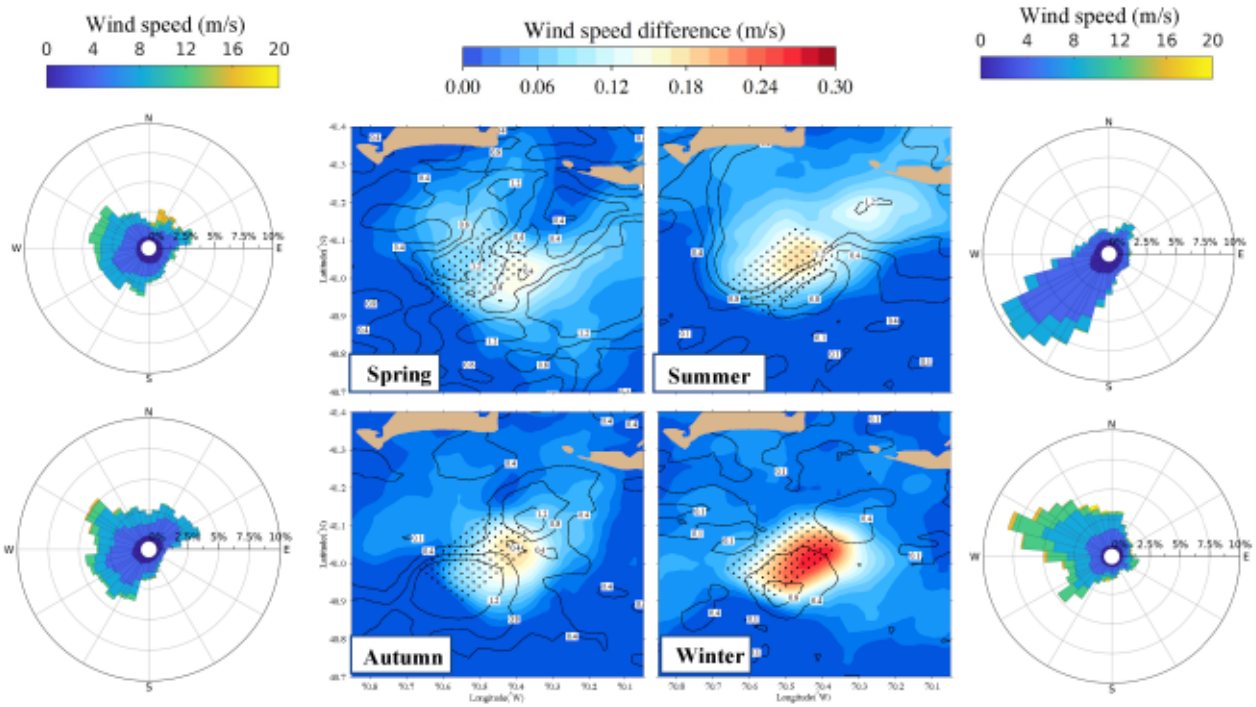

Fig. 14. Seasonally averaged changes in wind speed (images) and directions (contours) due to wind turbines over 2013. The surrounding wind rose plots represent the wind intensity and frequency over spring (upper-left), summer (upper-right), autumn (lower-left), and winter (lower-right).

scallop larvae in the region, despite the flows in both scenarios pushing the larvae offshore towards the NLCA (Fig. 15). In both semidiurnal and diel migration behavior cases, the flow influenced by downwind wakes enhanced the larval convergence on their journeys to the NLCA, leading to a higher larval density in the eastern portion of the closed area. Meanwhile, as most scallop larvae originated from the closed area of the GSC, changes in the flow patterns due to downwind wakes significantly reduced southwestward larval transport during the fall. This was the reason for the lower density in the NLCA when accounting for the downwind wake effect. The alteration in wind speed caused by WTGs did not significantly impact the mixed layer depth, so most changes in larval transport were attributed to the variation in flow caused by downwind wakes.

3.2.3. *Comparison of D1 and D2 layout designs*

VW proposed two alternative layout designs (D1 and D2) within the lease area of OCS-A-0501, featuring a separation spacing of approxi-mately 0.75–1.0 nautical miles between individual WTGs. In the D1

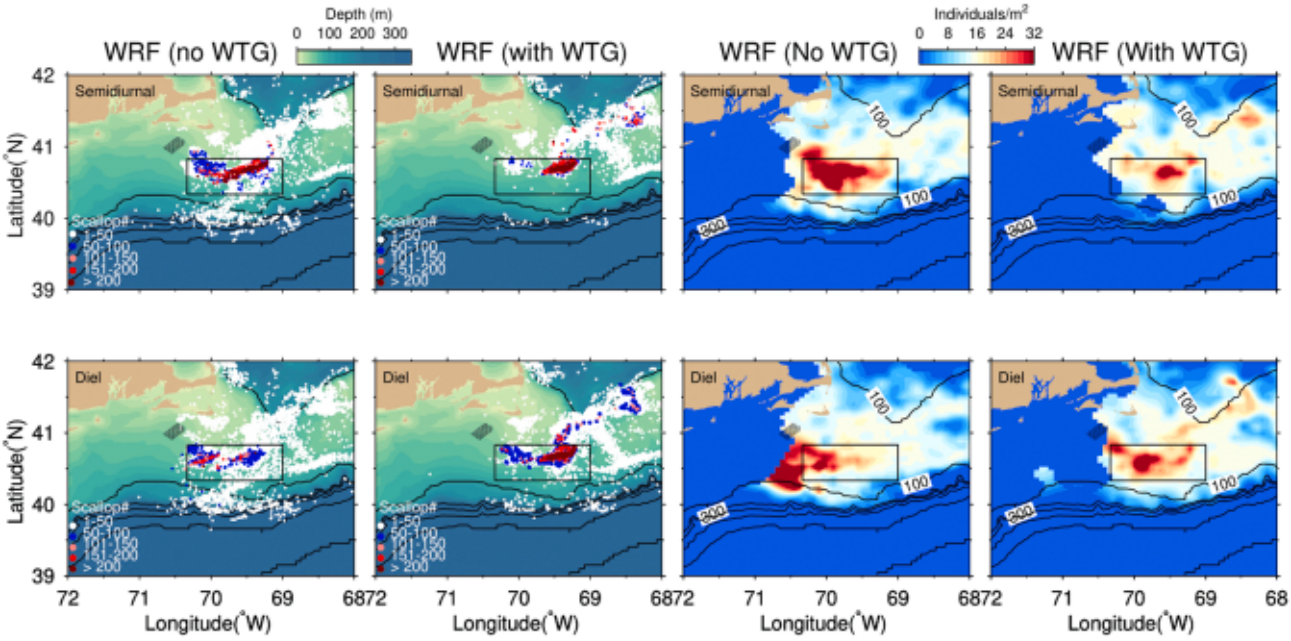

Fig. 15. Settlement locations of super-individual larvae (left panels) and densities (right panels) for the cases with and without considering the wind and heat flux changes due to wind turbines. The experiments were conducted from September to November 2013, considering diel and semi-diurnal larval migration in the mixed layer.

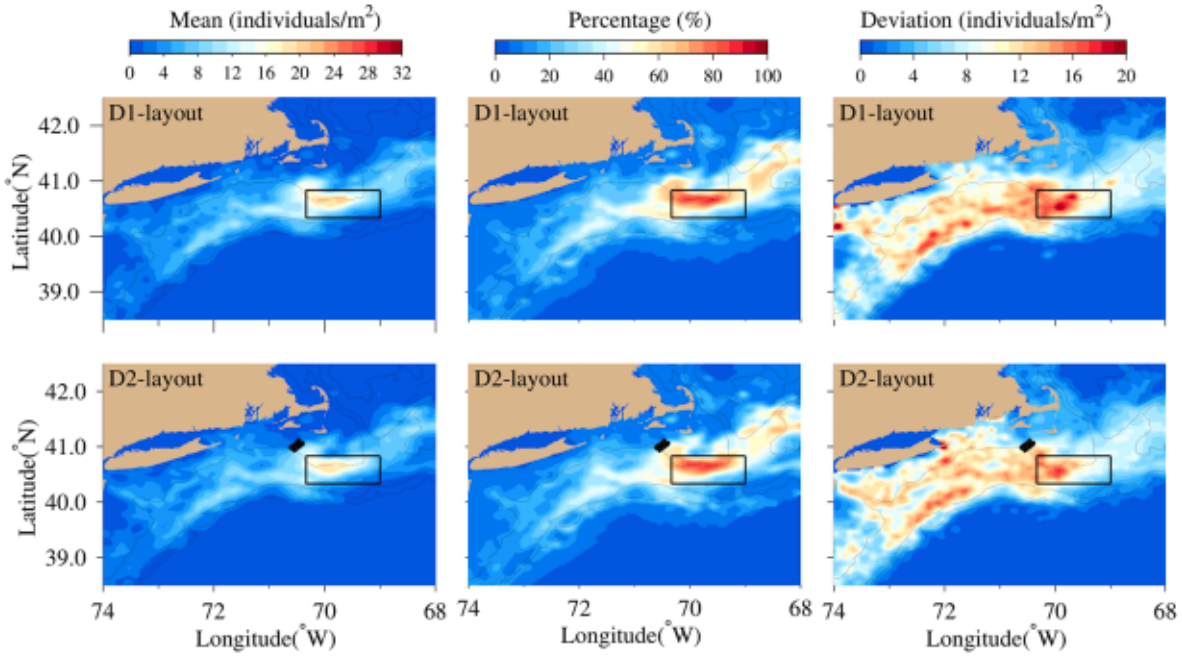

Fig. 16. The swimming behavior-ensembled, means, percentages, and standard deviations of settled scallop larvae over 2009. 2010 and 2013 for the D1- and D2-layout cases. Black lines are the 50, 100, and 200-m isobath contours. A black box is the Nantucket Lightship Closed Area (NLCA).

layout, WTGs follow a northwest-southeast orientation, while the D2 layout adopts an east–west alignment.

We conducted a comparative analysis of larval dispersions and settlements between the D1 and D2 layout designs for the years 2009, 2010, and 2013. For these cases, statistics analyses were performed to calculate ensemble larval swimming-averaged means, percentages, and deviations of settled scallop larvae. The ensemble considered all experiments with identical initial and boundary conditions, encompassing both diel and semi-diurnal larval swimming behaviors. The results indicated that the two alternative layout designs would not significantly influence the overall distribution of scallop larvae in the region, except for noticeable differences in larval abundance in the NLCA (Fig. 16). Both D1- and D2-layout arrangements could considerably alter the flow field and enhance offshore water transport. Interestingly, these changes were not markedly influenced by the orientation of WTGs' layout.

3.2.4. Impact of regional warming on scallop larval transport considering the presence of WTGs

Warming is anticipated to increase vertical stratification and reduce the OML depth. This study explores the impact of warming on scallop

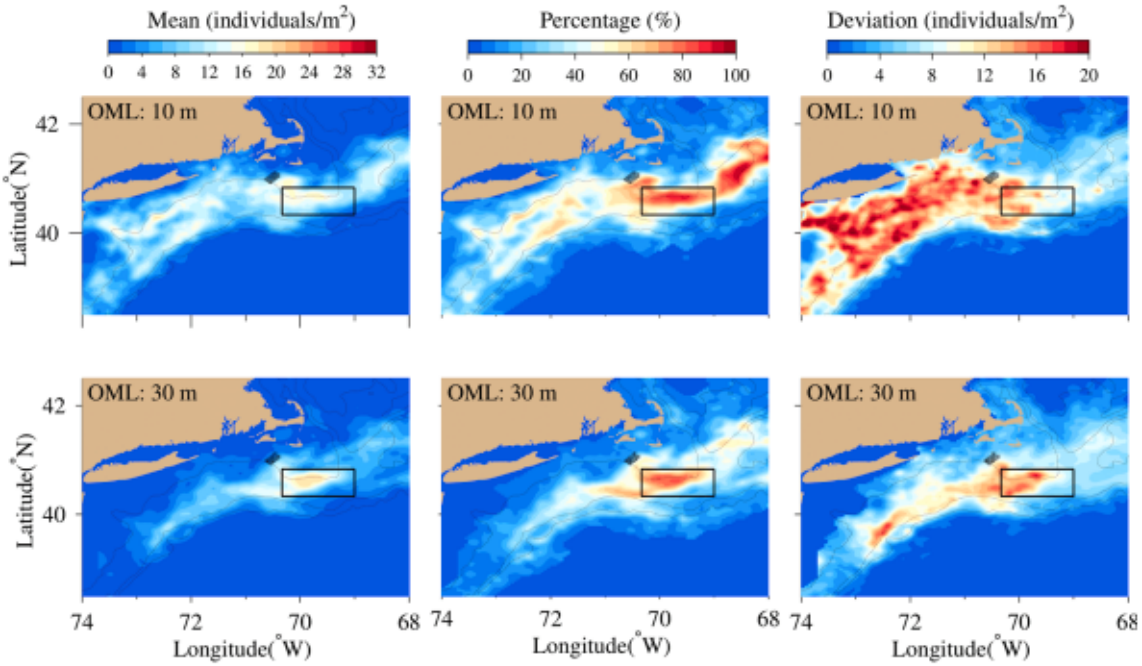

Fig. 17. The swimming behavior-ensembled, means, percentages, and standard deviations of settled scallop larvae over 2009, 2010, and 2013 for the 10- (upper panels) and 30-m (lower panels) OML cases. The ensemble considers both the D1- and D2-layout monopile arrangements. Black lines are the 50, 100, and 200-m isobath contours. The black box is the Nantucket Lightship Closed Area (NLCA).

larval transport under the influence of WTGs by comparing two experimental scenarios with different OML depths, specifically 10 and 30 m.

Wang (2023) projected changes in sea surface temperature (SST) in the US Northeast region through downscaled regional climate experiments using WRF and FVCOM. The results indicated a projected increase of approximately 2.5 °C in SST by 2050 compared to the present. This finding is about 1.0 °C higher than the projection by the Bedford Institute of Oceanography North Atlantic Model (BNAM) (Brickman et al., 2021), but aligns with the 2.25–2.75 °C projection by the Regional Ocean Modeling System (ROMS) (Brickman et al., 2021).

The downscaled regional climate WRF and FVCOM experiments suggest that warming significantly increases water stratification in the

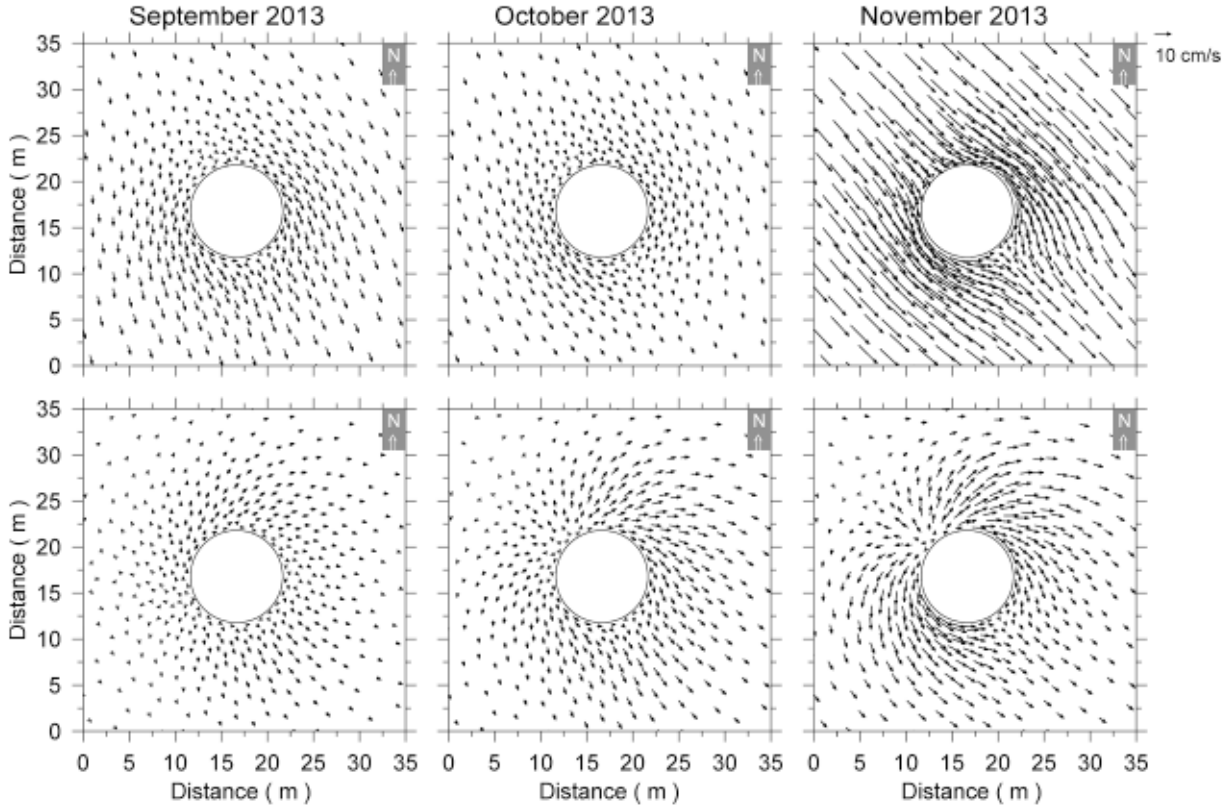

Fig. 18. Monthly-averaged currents at the surface (upper) and bottom (lower) for the case with wind turbines for September, October, and November 2013.

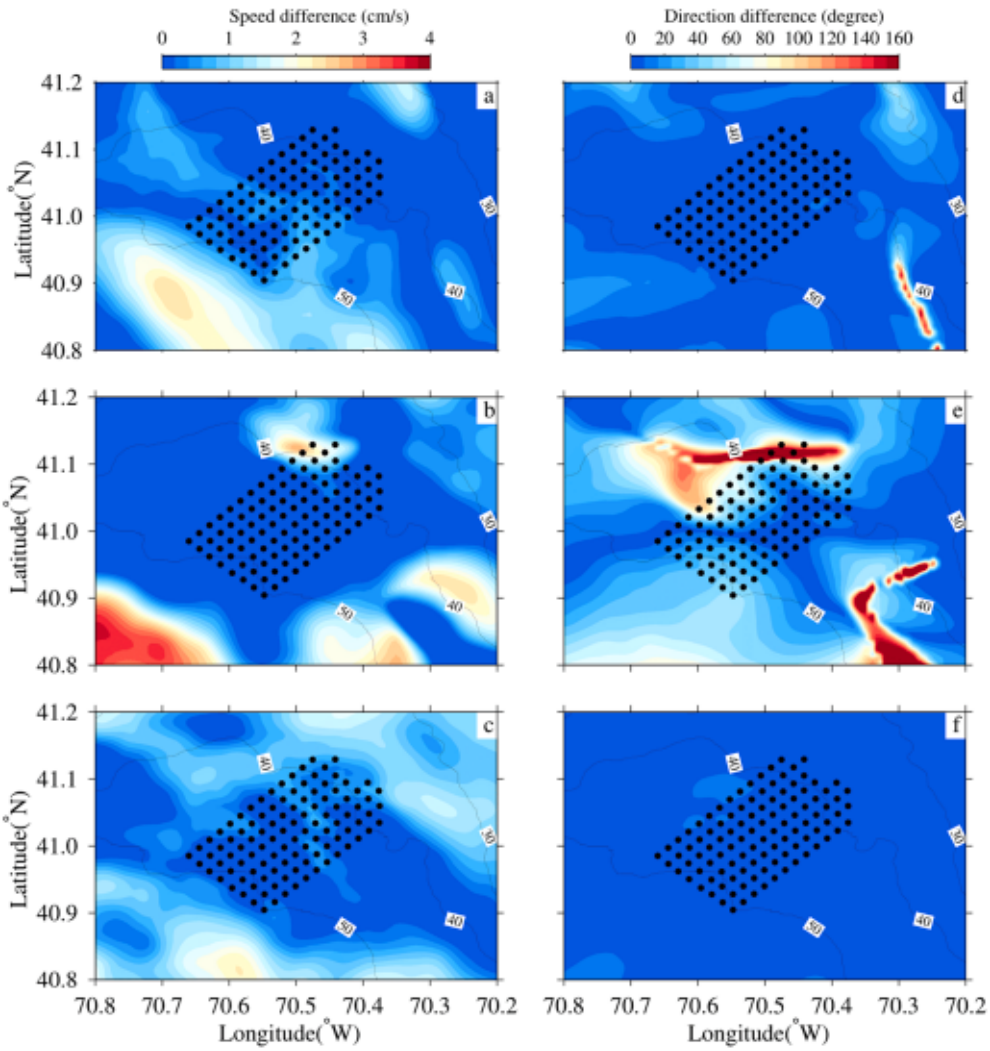

Fig. 19. Monthly-averaged flow speed (left panels) and direction (right panels) differences around the WTG array between the cases with and without wind turbines for September, October, and November 2013. Black dots: turbine locations.

U. S Northeast region during spring through summer. Under a warming condition, OML depths vary in a range of 10–30 m over the southern NES during fall (Chen et al., 2021a; Wang, 2023). We consider the 10-m OML case as an intensive warming scenario and the 30-m OML case as a moderate warming scenario. The experiments were conducted using the flow field produced by the 2009, 2010, and 2013 simulations with WTGs, taking into account both the diel and semi-diurnal larval swim-ming behaviors.

The distributions of ensemble larval swimming-averaged means, percentages, and deviations of settled scallop larvae for the 30-OML case resemble those shown with WTGs in Fig. 13 (Fig. 17). When the OML depth reduced to 10 m, the scallop larvae moved significantly onshore, southward, and northward. A large percentage of scallop larvae could settle around the WTGs' area (Fig. 17). The reduction in OML depth due to warming could enhance the interannual variability of scallop larval dispersal and settlement over the southern NES. This result suggests that as warming continues, the impact of offshore wind farms on scallop larval transport could exhibit significant international variability.

4. Discussions

The comparison of the scallop larval movement between the cases with and with WTGs suggests that installing a WTG array in the lease area of OCS-A-0501 could enhance the offshore water transport over Nantucket Shoal. Such change in flow is mainly attributed to the cu-mulative effects of the mesoscale flow around individual WTGs.

We calculated the 40-h low-pass filtered currents and their difference for the cases with and without WTGs. The result indicates that fluid- monopile interactions generate a net offshore mesoscale flow around individual WTGs (Fig. 18). Under stratified conditions, this low- frequency subtidal flow varies significantly with depth. In 2013, for instance, the monthly average subtidal flow around individual WTGs in September through November was southeastward near the surface and northeastward near the bottom. The monthly subtidal flow around WTGs was approximately 2–3 cm/s in September and October, but it increased to ~ 10 cm/s in November. This flow directed the scallop larvae offshore in the WTG areas.

The local monopile-fluid interaction significantly influenced the low- frequency subtidal flow within and around WTGs. We calculated the monthly-averaged 40-hour low-passed, near-surface flow difference between the cases with and without WTGs for September, October, and November 2013 (Fig. 19). In September, the speed difference varied around the WTG array, reaching larger values (up to ~ 2–3 cm/s) in the southwestern area and smaller values in the northeastern region. However, the flow direction difference was significant, up to 100° in the offshore area around 40-m isobath. In October, the most considerable speed difference occurred in the northwestern corner of the WTG array and around the 50-m isobath, with a maximum difference of ~ 3–5 cm/

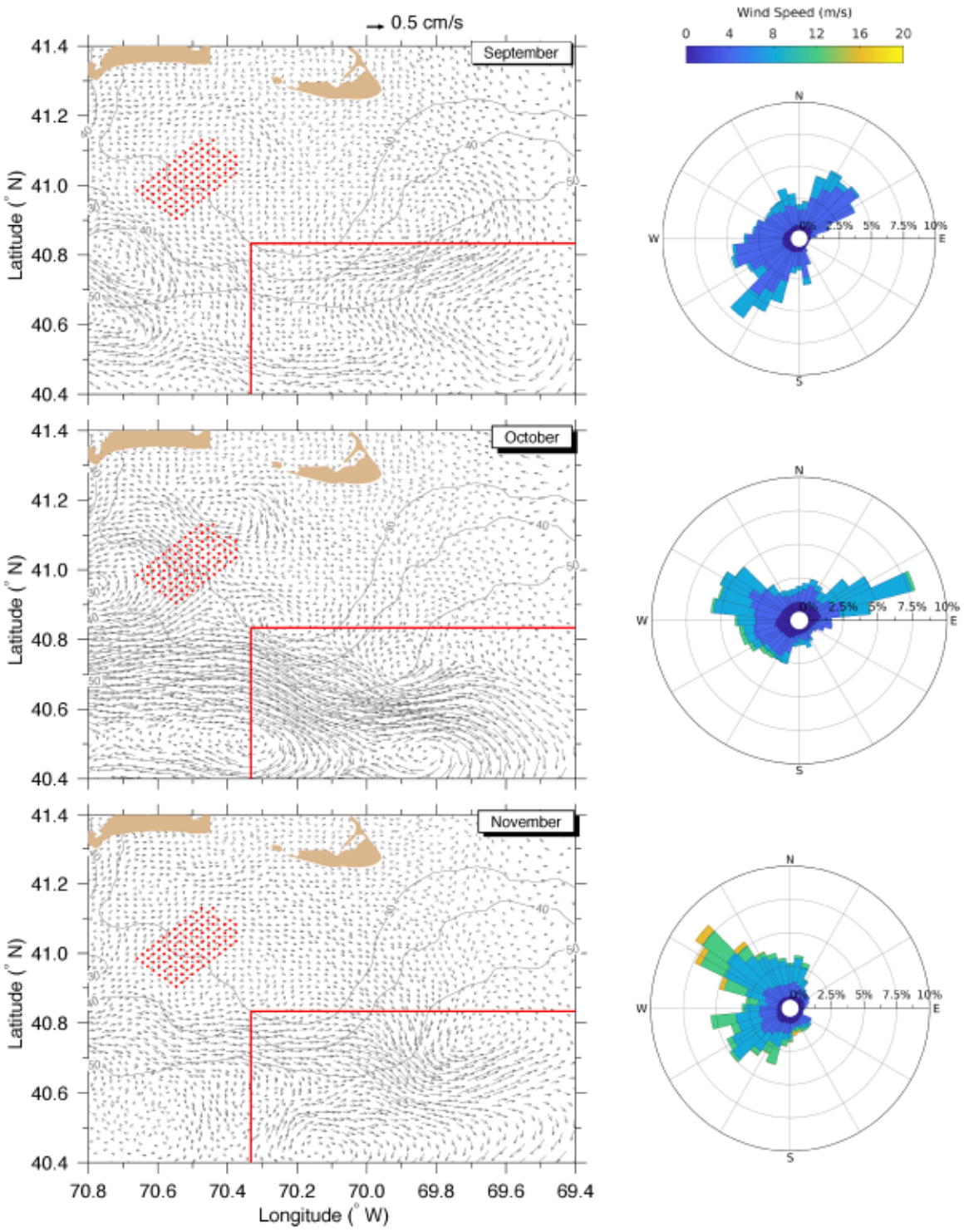

Fig. 20. Left panels: monthly-averaged flow differences between the cases with and without wind turbines over Nantucket Shoal for September, October, and November 2013. Red line: the boundary of the NLCA. Red dots: the monopile's location. Left panel: the rose maps of the wind intensity and frequency over September (upper), October (middle), and November (lower). (For interpretation of the references to color in this figure legend, the reader is referred to the web version of this article.)

s. The current direction difference reached 120-160° in the region of significant flow change. In November, a substantial change in flow speed occurred on the northeastern and southwestern sides of the WTG array, even though the flow direction change was less than 10°.

We further examined the regional-scale low-frequency subtidal flow changes over Nantucket Shoal, discovering that these changes varied with the wind intensity and direction. The most substantial flow change occurred around the 40 to 50-m isobath region (Fig. 20), consistent with the temperature difference observed between the cases with and without GTWs (Fig. 11). To visualize the velocity changes on a regional scale, we plotted the monthly-averaged subtidal flows with a 2.0-km horizontal resolution. In September, varying wind directions, with a higher per-centage from the northeast or southwest, intensified the anticyclonic subtidal flow around the 40 to 50-m isobaths in the southwestern area of

the WTG array. This created an eastward flow toward and inside the NLCA, enhancing the anticyclonic eddy inside the NLCA and strengthening the local scallop larval retention. In October, the northwesterly and northeasterly winds prevailed. The downwind wake due to WTGs generated an anticyclonic eddy in the northeastern area at the outer edge of WTGs and a cyclonic vortex in the southeastern region in the WTG array. The eastward flow and anticyclonic eddy around the 40 to 50-m isobaths and inside the NLCA were significantly intensified, with speeds potentially ~ 5.0 cm/s or greater. In November, the dominance of northwesterly winds, especially during storms with speeds up to ~ 15 m/s, led to the disappearance of eddies around the WTG array. However, the eastward flow toward the NLCA on the 40 to 50-m isobaths still persisted, albeit weaker than in October.

Similar changes in the subtidal flow were also observed during September through November in 2009 and 2010. It suggested that regardless of variations in wind intensity and direction, the downwind wake caused by the WTG array could consistently produce and enhance offshore water transport, particularly around the 40 to 50-m isobaths. This phenomenon explains the observed offshore shift of scallop larvae and their accumulation in the NLCA when the WTGs were included in the model.

It is important to note that our modeling experiments focused solely on one wind farm development site within the lease area of OCS-A-0501. However, there are eight other lease areas in MA and RI waters where offshore wind farm development is ongoing. According to the updated Construction and Operation Plans (COPs) obtained from the nine offshore wind companies, approximately 962 WTGs are slated for deployment, with a separation scale of 1.0 by 1.0 nautical miles in the region (information received through personal communication with Dr. Gregory DeCelles at Orsted). As the spatial scale of offshore wind extends, the cumulative impacts of WTGs on scallop larval dispersion and transports could undergo significant changes. To offer model projections for the New England Fishery Management Council regarding the changing marine environment due to the regional wind farm development, it is imperative to conduct assessments considering all leased areas in MA and RI waters. Our current modeling experiments have demonstrated the effectiveness of the coupled Scallop-IBM and NS-FVCOM/NECOFS model system in resolving mesoscale flow and mixing generated by an offshore wind farm. By nesting NS-FVCOM with NECOFS, this model system can also be utilized to examine the broader impact of the offshore wind farm development on regional scallop larval dispersal and settlement. This comprehensive approach is crucial for understanding the cumulative effects and potential ecological implications of multiple wind farms across the entire region.

We conducted numerical experiments using NS-FVCOM under the hydrostatic approximation. In cases where the vertical-to-horizontal scale ratio is in O(1), nonhydrostatic processes may play a crucial role in generating high-frequency internal waves due to fluid-monopile interactions and vertical convection caused by extreme surface cooling during storms. NS-FVCOM demonstrated that fluid-monopile interactions produced high-frequency internal waves with a period of approximately 1.0 h around individual monopiles. However, it is worth noting that the frequencies of these waves may differ when nonhydrostatic processes are considered. Meanwhile, the hydrostatic model tended to exaggerate the maximum vertical viscosity during storms.

To gain a comprehensive understanding, further examination should be undertaken to quantify the contributions of non-hydrostatic process-induced high-frequency internal waves and convection. This analysis will help elucidate the impact of these processes on changes in water transport and stratifications induced by WTGs.

5. Summaries and conclusions

A high-resolution model, with a grid resolution of up to ~ 1.0 m, was developed to couple a wind turbine-resolving hydrodynamical model (NS-FVCOM) with an individual-based scallop model (Scallop-IBM). This coupled model aims to evaluate the potential impact of offshore wind renewable energy facilities on the local and regional circulation, stratification, and dispersal and settlement of scallop larvae in the U.S. Northeast. Within the turbine array, a body-fitted grid was employed to meticulously resolve each monopile and its consequent influence on flow fields and turbulent mixing. As a pilot site, we focused on the Vineyard Wind lease area (OCS0A-0501). Our examination involved assessing changes in the flow field, mixing via stratification, and their effects on scallop larval transport and settlement over the southern NES. The model simulations took into account variations in wind and heat flux changes caused by WTGs, two layout designs, and projected climate change scenarios.

The primary results indicate that within the M_2 tidal currents-dominant and stratified Nantucket Shoal, the interaction of tidal currents with monopiles produces intricate patterns of horizontal flow shear on the lee side. The mesoscale currents, induced by fluid–structure interaction, deviate significantly from the idealized flow fields typically examined in the device-scale laboratory or coarse-grid hydrodynamical models with subgrid-scale explicit parametrizations.

Stratification played a crucial role in altering the flow around individual WTGs throughout the water column. The maximum bottom stress is primarily oriented in the onshore-offshore direction, and vertical eddy viscosity is observed throughout the water column around all directions of individual WTGs. The weakening of vertical stratification, resulting from enhanced mixing around monopiles, is mainly confined to the wind farm development area.

The local monopile-fluid interaction can intensify the offshore low-frequency subtidal flow around 40 to 50-m isobaths, forming mesoscale eddies over the shelf. This enhanced offshore water transport leads to the displacement of scallop larvae offshore towards the NLCA. The accumulation of larvae in the NLCA is primarily attributed to eddy-induced retention.

CRediT authorship contribution statement

Changsheng Chen: Writing – review & editing, Writing – original draft, Supervision, Project administration, Methodology, Investigation, Funding acquisition, Formal analysis, Conceptualization. **Liuzhi Zhao:** Validation, Formal analysis. **Huichan Lin:** Methodology. **Pingguo He:** Project administration, Investigation. **Siqi Li:** Software, Methodology. **Zhongxiang Wu:** Validation, Software, Formal analysis. **Jianhua Qi:** Software. **Qichun Xu:** Software. **Kevin Stokesbury:** Project administration, Investigation. **Lu Wang:** Investigation.

Declaration of competing interest

The authors declare that they have no known competing financial interests or personal relationships that could have appeared to influence the work reported in this paper.

Data availability

No data was used for the research described in the article.

Acknowledgments

We gratefully acknowledge the funds provided by the NOAA RSA Program with grant numbers NA19NMF-4540023 and NA22NMF4540046, supporting C. Chen, L. Zhao, P. He, and K. Stokesbury. The NECOFS product, supported by the NOAA-funded IOOS NERACOOS program, was created under subcontract numbers NA16NOS0120023 and NA21NOS 0120095. Additionally, NECOFS improvements were partly funded by the NSF LTER Program through WHOI subcontract number A101636/82267610.

Our sincere thanks go to the Canadian Department of Fisheries and Oceans (DFO) for generously providing the Canadian scallop survey

dataset. We are particularly grateful to Jessica Sameoto and Freya Keyser at DFO for their invaluable assistance in creating and delivering a well-organized scallop dataset. Special appreciation is also extended to Dr. Deborah Hart and other NOAA scientists for making the NOAA dredge survey dataset available for this study and Dr. DeCelles at Orsted for providing the updated Construction Operation Plan of the offshore wind farm development in MA and RI waters.

References

Beardsley, R.C., Chen, C., Xu, Q., 2013. Coastal flooding in Scituate (MA): a FVCOM study of the Dec. 27, nor'easter. J. Geophys. Res.-Oceans 118. https://doi.org/10.1002/2013JC008862.

Bergström, L., Sundqvist, F., Bergström, U., 2013. Effects of an offshore wind farm on temporal and spatial patterns in the demersal fish community. Mar. Ecol. Prog. Ser. 485, 199–210.

Brickman, D., Alexander, M.A., Pershing, A., Scott, J.D., Wang, Z., 2021. Projections of physical conditions in the Gulf of Maine in 2050. Elementa: Sci. Anthrop. 9 (1), 00055.

Carey, D.A., Wilber, D.H., Read, L.B., Guarinello, M.L., Griffin, M., Sabo, S., 2020. Effects of the Block Island Wind Farm on Coastal Resources. Oceanography 33 (4), 70–81. Chang, P.K., 1970. Separation of flow. Pergamon Press, p. 777.

Chen, C., Beardsley, R.C., Luettich Jr, R.A., Westerink, J.J., Wang, H., Perrie, W., Xu, Q., Dohahue, A.S., Qi, J., Lin, H., Zhao, L., Kerr, P., Meng, Y., Toulany, B., 2013b. Extratropical storm inundation testbed: intermodal comparisons in Scituate, Massachusetts. J. Geophys. Res. 118 https://doi.org/10.1002/jgrc.20397.

Chen, C, R. C. Beardsley, and G. Cowles, 2006. An unstructured grid, finite-volume coastal ocean model (FVCOM) system. Special Issue entitled "*Advance in Computation*al *Oceanography*," *Oceanography*, 19(1), 78-89.

Chen, C., Huang, H., Beardsley, R. C., Xu, Q., Limeburner, W. Cowles, G. W., Sun, Y., Qi, J., Lin, H., 2011. Tidal dynamics in the Gulf of Maine and New England Shelf: An application of FVCOM. *J. Geophys. Res.*-Oceans 116, C12010, doi: 10.1029/2011 JC007054.

Chen, C., Beardsley, R. C., Cowles, G., Qi, J., Lai, Z., Gao, G., Stuebe, D., Liu, H., Xu, Q., Xue, P., Ge, J., Ji, R., Hu, S., Tian, R., Huang, H., Wu, L., Lin, H., Sun, Y., Zhao, L., 2013a. An unstructured-grid, finite-volume community ocean model FVCOM user manual (4th edition), *SMAST/UMASSD Technical Report-13-0701*, University of Massachusetts-Dartmouth, pp 404.

Chen, C., Beardsley, R. C., Qi, J., Lin, H., 2016a. Use of Finite-Volume Modeling and the Northeast Coastal Ocean Forecast System in offshore wind energy resource planning. Final Report to the U.S. Department of the Interior, Bureau of Ocean Energy Management, Office of Renewable Energy Programs. BOEM 2016-050. 131pp.

Chen, C. Zhao, L., Gallager, S. Ji, R., He, P., Davis, C., Beardsley, R. C., Hart, D., Gentleman, W. C., Wang, L., Li, S., Lin, H., Stokesbury, K., Bethoney, D., 2021a. Impact of larval behaviors on dispersal and connectivity of sea scallop larvae over the northeast U.S. shelf. *Progress in Oceanography*, 195, 102604, Doi: 10.1016/j. pocean. 2021.102604.

Chen, C., Zhao, L., He, P., Beardsley, C. R., Gallager, S., Stokesbury, K, 2021b. Assessing potential impacts of offshore wind facilities on regional sea scallop larval and early juvenile transports. A short report for the 2021 Scallop RSA Share Day, May 6 and 12, 2021,19pp.

Chen, C., Liu, H., Beardsley, R.C., 2003. An unstructured, finite-volume, three-dimensional, primitive equation ocean model: application to coastal ocean and estuaries. J. Atmos. Oceanic Tech. 20, 159–186.

Chen, C., Gao, G., Zhang, Y., Beardsley, R.C., Lai, Z., Qi, J., Lin, H., 2016. Circulation in the Arctic Ocean: Results from a high-resolution coupled ice-sea nested Global-FVCOM and Arctic-FVCOM system. Prog. Oceanogr. 141 (2016), 60–80. https://doi. org/10.1016/j.pocean.2015.12.002.

Chen, C., Lin, Z., Beardsley, R.C., Shyka, T., Zhang, Y., Xu, Q., Qi, J., Lin, H., Xu, D., 2020. Impacts of sea-level rise on future storm-induced coastal inundation over Massachusetts Coast. Natural Hazard. https://doi.org/10.1007/s11069-020-04467-x.

Cowles, G., Lentz, S.J., Chen, C., Xu, Q., Beardsley, R.C., 2008. Comparison of observed and model-computed low-frequency circulation and hydrography on the New England Shelf. J. Geophys. Res. 113, C09015. https://doi.org/10.1029/ 2007JC004394.

Cragg, S.M., 2006. Development, physiology and ecology of scallop larvae. In: Shumway, S.E., Parsons, G.J. (Eds.), Scallops: *Biology, Ecology and Aquaculture*. Elsevier, Amsterdam, pp. 45–122.

Culliney, J.L., 1974. Larval development of the giant sea scallop Placopecten magellanicus (Gmelin). Biol. Bull. 147, 321–332.

Davies, K.T.A., Gentlemen, W.C., DiBacco, C., Johnson, C.L., 2015. Fisheries closed area strengthen scallop larval settlement and connectivity among closed areas and across international open fishing grounds: a model study. Environ. Manag. 16. https://doi. org/10.1007/s00267-015-0526-9.

DiBacco, C., Robert, G., Grant, J., 1995. Reproductive cycle of the sea scallop, Placopecten magellanicus (Gmelin, 1791), on northeast-ern Georges Bank. J. Shellfish Res. 14, 59–69.

Fitch, A., Olson, J.B., Lundquist, J.K., Dudhia, J., Gupta, A.K., Michalakes, J., 2012. Local and mesoscale impacts of wind farms at parameterized in a mesoscale NWP model. Mon. Weather Rev. 140, 3017–3038.

Gallager, S.M., 1993. Hydrodynamic disturbances produced by small zooplankton: a case study for veliger larvae of bivalve molluscs. J. Plankton Res. 15 (11), 1277–1296.

Gallager, S.M., Manuel, J.L., Manning, D.A., O'Dor, R., 1996. Ontogenetic changes in the vertical distribution of scallop larvae *Placopecten megellanicus* in 9 m-deep mesocosms as a function of light, food, and temperature stratification. Mar. Biol. 124, 679–692.

Grell, G.A., 1993. Prognostic Evaluation of Assumptions Used by Cumulus Parameterizations. Mon. Wea. Rev. 121, 764–787.

Hart, D.R., 2006. Effects of sea stars and crabs on sea scallop Placopecten magellanicus recruitment in the Mid-Atlantic Bight (USA). Mar. Ecol. Prog. Ser. 306, 209–221. Hart, D. R., Chute, A. S., 2004. Essential Fish Habitat Source Document: Sea Scallop, *Placopecten magellanicus*, Life History and Habitat Characteristics, 2nd Ed. NOAA Tech. Mem. NMFS-NE-189.

Hart, D.R., Rago, P.J., 2006. Long-term dynamics of U.S. Atlantic sea scallop *Placopecten magellanicus* populations. N. Am. J. Fish. Manag. 26, 490–501. https://doi.org/ 10.1577/M04-116.1.

Johnson, T. L., J. J. Jon van Berkel, L. O. Mortensen, M. A. Bell, I. Tiong, B. Hernandez, D. B. Snyder, F. Thomsen, O. S. Petersen, 2021. Hydrodynamic Modeling, Particle Tracking and Agent-Based Modeling of Larvae in the U.S. Mid-Atlantic Bight. Lakewood (CO): US Department of the Interior, Bureau of Ocean Energy Management. OCS Study BOEM 2021-049. 232 p.

Larsen, P.F., Lee, R.M., 1978. Observations on the abundance, distribution and growth of postlarval sea scallop, *Placopeten magellanicus*, on Georges Bank. The Nautilus 92, 112–116.

Lentz, S.J., 2017. Seasonal warming of the Middle Atlantic Bight Cold Pool. J. Geophys. Res. Oceans 122, 941–954. https://doi.org/10.1002/2016JC01220.

Lentz, S.J., Shearman, R.K., Anderson, S., Plueddemann, A., Edson, J., 2003. Evolution of stratification over the New England Shelf during the Coastal Mixing and Optics Study, August 1996 - June 1997. J. Geophys. Res. 108 (C1), 3008. https://doi.org/ 10.1029/2001JC001121.

Li, S., Chen, C., 2022. Air-sea Interaction Processes during Hurricane Sandy: Coupled WRF-FVCOM Model Simulation. Prog. Oceanogr. 206, 102855 https://doi.org/ 10.1016/j.pocean.2022.102855.

Li, S., Chen, C., Wu, Z., Beardsley, R. C., Li, M., 2020. Impacts of oceanic mixing layer on hurricanes: a simulation experiment with Hurricane Sandy. *Journal of Geophysical Research-Oceans*, 125, e2019JC015851. https://doi.org/10.1029/2019JC015851.

Li, Y., Fratantoni, P.S., Chen, C., Hare, J., Sun, Y., Beardsley, R.C., Ji, R., 2015. Spatia-temporal patterns of stratification on the Northwest Atlantic shelf. Prog. Oceanogr. 134, 123–127.

Manuel, J.L., Gallager, S.M., Pearce, C.M., Manning, D.A., O'Dor, R.K., 1996. Veligers from different populations of sea scallop Placopecten magellanicus have different migration patterns. Mar. Ecol. Prog. Ser. 142, 147–163.

Melvin, G. D., Dadswell, M. J., Chandler, R. A., 1985. Movement of scallop (*Placopecten magellaniucs*) (Gmelin, 1791) (Mol-lusca: Pectinidae) on Georges Bank. *Can. Atl. Fish. Sci. Advis. Comm. Res*. Doc. 95.

Miles, T., Murphy, S., Kohut, J., Borsetti, S., Munroe, D., 2021. Offshore wind energy and the Mid-Atlantic Bight cold pool: a review of potential interactions. Mar. Technol. Soc. J. 55 (4), 72–87.

Mullen, D.M., Morning, J.R., 1986. Species profiles: Life histories and environmental requirements of coastal fishes and invertebrates (North Atlantic) sea scallop. Biol. Rep. US Fish Wildlife Service 1986, 21p.

Naidu, K.S., Robert, G., 2006. Fisheries sea scallop. *Placopecten magellanicus*. In: Shumway, S.E., Parsons, G.J. (Eds.), Scallops: Biology, Ecology and Aquaculture. Elsevier, Amsterdam, pp. 869–905.

Northeast Fisheries Science Center (NFSC), 2018. 65th Northeast Regional Stock Assessment Workshop (65th SAW) Assessment Report. US Dept Commerce. Northeast Fish. Sci. Cent. Ref. Doc. 18–08, 43 pp.

OCS EIS/EA, BOEM2018-060: Vineyard Wind offshore wind energy project draft environmental impact statement, December 2018, U.S. Department of the Interior, Bureau of Ocean Energy Management, 478pp.

Pearce, C. M., J. L. Manuel, J. L., S. M. Gallager, S. M., D. A. Manning, D. A., R. K. O'Dor, R. K., Bourget, E., 2004. Depth and timing of settlement of veligers from different populations of giant scallop, *Placopecten magellanicus* (Gmelin), in thermally stratified mesocosms. *Journal of Experimental Marine Biology and Ecology* 312, 187-214.

Pearce, C.M., Gallager, S.M., Manning, D.A., O'Dor, R.K., Bourget, E., 1998. Effect of thermoclines and turbulence on depth of larval settlement and spat recruitment of the giant scallop *Placopecten magellanicus* larvae in 9 m-deep laboratory mesocosms. Mar. Ecol. Progr. Ser. 165, 195–215.

Posgay, J.A., 1976. Population assessment of the Georges Bank sea scallop stocks. ICES Document CM 1976/K, 34.

Posgay, J.A., 1981. Movement of tagged scallops on Georges Bank. Fish. Rev. 43, 19–25.

Posgay, J.A., Norman, K.D., 1958. An observation on the spawning of the sea scallop, Placopecten magellanicus (Gmelin), on Georges Bank. Limnol. Oceanogr. 3, 478.

Qi, J., Chen, C., Beardsley, R.C., Perrie, W., Cowles, G.W., Lai, Z., 2009. An unstructured-grid finite-volume surface wave model (FVCOM-SWAVE): implementation, validations and applications. Ocean Model. https://doi.org/10.1016/j. ocemod.2009.01.007.

Rillahan, C., He, P., 2021. Vineyard Wind Demersal Trawl Survey Annual Report – 501N Study Area. 2020/2021 Annual report. University of Massachusetts Dartmouth - SMAST, New Bedford, MA. SMAST-CE-REP2021-101. 196 pp. https://static1. squarespace.com/static /5a2eae32be42d64ed467f9d1/t/ 63178a469af5cb3e78939f91/1662487114729/SMAST_2020_2021_Annual_501N_ Trawl_Survey_Report_Final.pdf.

Schlichting, H., 1979. Boundary Layer Theory, 7th edition. McGraw-Hill, New York.

Shearman, R.K., Lentz, S.J., 2003. Dynamics of mean and subtidal flow on the New England Shelf. J. Geophys. Res. 108 (C8), 3281. https://doi.org/10.1029/ 2002JC001417.

Shearman, R.K., Lentz, S.J., 2004. Observations of tidal variability on the New England Shelf. J. Geophys. Res. 109 (C6), 6010. https://doi.org/10.1029/2003JC001972.

Shumway, S. E., Parsons, G. L. (eds.). 2016. *Scallops, Biology, Ecology, Aquaculture, and Fisheries*. Elsevier, Amsterdam, Oxford, and Cambridge. 1214 pp.

Stewart, P.L., Arnold, S.H., 1994. Environmental requirements of the sea scallop (Placopecten magellanicus) in eastern Canada and its response to human impacts. Can. Tech Rep. Fish. Aquat. Sci. 2005, 1–36.

Stokesbury, K.D.E., Bethoney, N.D., 2020. How many sea scallops are there and why does it matter? Front. Ecol. Environ. https://doi.org/10.1002/fee.2244.

Stokesbury, J. D., Cassidy, K., Lowery T. M., 2023. Constructing a baseline groundfish trawl survey for an offshore windfarm development area. *Marine and Coastal Fisheries*: *Dynamics, Management, and Ecosystem Sciences*, 15, e10267. https:/dou.org/10.1002/ mcfs.10267.

Sun, Y., Chen, C., Beardsley, R.C., Ullman, D., Butman, B., Lin, L., 2016. Surface circulation in Block Island Sound and adjacent coastal and shelf regions: A FVCOM-CODAR comparison. Prog. Oceanogr. 143 (2016), 26–45.

Sun, Y., Chen, C., Beardsley, R. C., Xu, Q., Qi, J.: Lin, H., 2013. Impact of current-wave interaction on storm surge simulation: A case study for Hurricane Bob. *J. Geophys. Res.-Oceans* 118, 2685-2701, doi:10.1002/jgrc.20207.

Tian, R.C., Chen, C., Stokesbury, K.D.E., Rothschild, B.J., Xu, Q., Hu, S., Cowles, G.W., Harris, B.P., Marino II, M.C., 2009a. Dispersal and settlement of sea scallop larvae spawned in the fishery closed areas on Georges Bank. ICES J. Mar. Sci. 66 (10), 2155–2164. https://doi.org/10.1093/icesjms/fsp175.

Tian, R.C., Chen, C., Stokesbury, K.D.E., Rothschild, B.J., Xu, Q., Cowles, G.W., Harris, B. P., Marino II, M.C., 2009b. Sensitivity analysis of sea scallop (Placopectenm agellanicus) larvae trajectories to hydrodynamic model configuration on Georges Bank and adjacent coastal regions. Fish. Oceanogr. 18, 173–184.

Tian, R.C., Chen, C., Stokesbury, K.D.E., Rothschild, B.J., Cowles, G.W., Xu, Q., Harris, B. P., Marino II., M.C., 2009c. Modeling the connectivity between sea scallop populations in the Middle Atlantic Bight and over Georges Bank. Mar. Ecol. Prog. Ser. 380, 147–160.

Tremblay, M.J., Sinclair, M., 1990a. Sea scallop larvae Placopecten magellanicus on Georges Bank: Vertical distribution in relation to water column stratification and food. Mar. Ecol. Prog. Ser. 61 (1–2), 1–15. https://doi.org/10.3354/meps061001.

Tremblay, M.J., Sinclair, M., 1990b. Diel migration of sea scallop larvae Placopecten magellanicus in a shallow embayment. Mar. Ecol. Prog. Ser. 67, 19–25.

Tremblay, M.J., Loder, J.W., Werner, F.E., Naimie, C.E., Page, F.H., Sinclair, M.M., 1994. Drift of sea scallop larvae *Placopecten magellanicus* on Georges Bank: a model study of the roles of mean advection, larval behavior and larval origin. Deep-Sea Res. II 41, 7–49.

Underwood, A.J., 1991. Beyond BACI: experimental designs for detecting human environmental impacts on temporal variations in natural populations. Mar. Freshw. Res. 42 (5), 569–587.

Van Hal, R., Griffioen, A.B., Van Keeken, O.A., 2017. Changes in fish communities on a small spatial scale, an effect of increased habitat complexity by an offshore wind farm. Mar. Environ. Res. 126, 26–36.

Wang, L., 2023. Simulating ocean acidification in the northeast U.S. region using a fully coupled three-dimensional biogeochemistry and ecosystem model. University of Massachusetts, p. 278 pp.. Ph.D. dissertation.

Wilber, D. H., Brown, L., J., Griffin, M., Carey, D. A., 2024. American lobster Homarus americanus responses to construction and operation of an offshore wind farm in southern New England. Mar. Ecol. Prog. Ser., 727, 123-142. Doi: 10.3354/meps14482.

Zhang, Y., Chen, C., Beardsley, R.C., Gao, G., Lai, Z., Curry, B., Lee, C.M., Lin, H., Qi, J., Xu, Q., 2016a. Studies of the Canadian Arctic Archipelago water transport and its relationship to basin-local forcings: Results from AO-FVCOM. J. Geophys. Res.-Oceans 121. https://doi.org/10.1002/2016JC011634, 121.

Zhang, Y., Chen, C., Beardsley, R.C., Gao, G., Qi, J., Lin, H., 2016b. Seasonal and interannual variability of the Arctic sea ice: a comparison between AO-FVCOM and observations. J. Geophys. Res.-Oceans 121. https://doi.org/10.1002/2016JC011841.

Zhang, Y., Chen, C., Beardsley, R.C., Perrie, W., Gao, G., Zhang, Y., Qi, J., Lin, H., 2020a. Applications of an unstructured grid surface wave model (FVCOM-SWAVE) to the Arctic Ocean: The interaction between ocean waves and sea ice. Ocean Model. 145, 101532 https://doi.org/10.1016/j.ocemod.2019.101532.

Zhang, Z., Chen, C., Beardsley, R.C., Li, S., Xu, Q., Song, Z., Zhang, D., Hu, D., Guo, F., 2020b. A FVCOM study of the potential coastal flooding in Apponagansett Bay and Clark Cove, Dartmouth Town (MA). Natural Hazard. https://doi.org/10.1007/s11069-020-04102-9.